THE MERCURY ATMOSPHERE

D. M. HUNTEN
University of Arizona

T. H. MORGAN
NASA Johnson Space Center

and

D. E. SHEMANSKY
University of Arizona

The known gases in Mercury's atmosphere are H, He and O, discovered by the ultraviolet spectrometer on Mariner 10, and Na and K, discovered from the ground by Potter and Morgan. Dayside number densities at the planet's surface are estimated to be between 100 and 4×10^4 cm^{-3}, with probable large nightside enhancements for hydrogen and helium. Other possible gases are considered; the only ones likely to be present in comparable abundance are H_2 and H_2O. The atmosphere is technically an exosphere, but the gas-surface interaction is very different from the interaction of a normal exosphere with the atmosphere below. Quantum-mechanical effects alter the velocity distribution and the rate of migration across the surface, and accommodation to the local temperature is inefficient. Probable sources are the solar wind for hydrogen and helium, and evaporation of meteoroidal material for the alkalis and water, with a possible contribution to the former by sputtering and photosputtering. Solar-wind ions generally do not enter the atmosphere directly, but rather via Mercury's magnetosphere. They tend to be implanted in surface materials, and later be displaced to the atmosphere by the impact of subsequent ions; most hydrogen is probably released as H_2. The dominant sink for all of the atoms seems to be photoionization. Following photoionization, most ions are recycled to the sur-

face and neutralized, although a significant fraction are swept up in the flows of the magnetosphere and solar wind. For H_2O photodissociation dominates, and may be a substantial source of H, H_2 and O. Solar radiation pressure is a large effect, especially for Na and K, but its role as a sink is probably small except for unusually fast atoms.

I. INTRODUCTION AND OVERVIEW

The atmosphere of Mercury is tenuous; the gas particle density is low enough that the planet's surface forms the exobase boundary. In other words, atoms collide with the surface more often than with each other. Five elements are known to be present in the atmosphere: oxygen, sodium, helium, potassium, and hydrogen, in order of decreasing abundance. Helium, hydrogen, and oxygen were discovered by the Mariner 10 airglow spectrometer (Broadfoot et al. 1974,1976), while sodium and potassium were discovered with groundbased instrumentation (Potter and Morgan 1985,1986*a*). In all cases, the basis of the identification was the observation of emission by resonant scattering of sunlight. Table I contains wavelengths, flux, subsolar point density, scale height and other observational details for each known constituent, as well as similar information for the Moon. We cannot say that these five elements constitute a complete list of the major species in the atmosphere of Mercury, because the total pressure of the known species is almost two orders of magnitude less than the upper limit of the atmospheric pressure, 10^{-12} bar, set by the Mariner 10 occultation experiment. Table II contains the measured upper limits of abundances and densities for other possible species at the location of the planet's terminator. The relationship between the data shown in Tables I and II is uncertain because little is known about the distribution of the gases over the surface. Limited observational evidence and uncertain atmospheric theory both suggest a large concentration of gases on the night side; the transition between night and day side in the terminator region is even less understood.

The physical quantities listed in Table I provide only a very schematic description of the atmosphere of Mercury, and much is unknown. The mean free path of an atom in Mercury's atmosphere is greater than the scale height of any of the components so that the atoms of the gas move on ballistic trajectories. The first collision experienced by a typical atom in the atmosphere is with the surface. The velocity distribution and extent of the atmosphere are controlled by poorly understood gas-surface interactions and velocity-dependent loss processes.

Early work on the lunar and Mercurian atmospheres, discussed in Sec. V, assumed that the gas-surface interaction could be represented in the same way as a true exobase, the level in an atmosphere above which collisions between atoms can be considered negligible. Although this assumption is invalid, it still serves as a useful point of departure. An exobase is not a true boundary;

TABLE I
Known Gases on Mercury and Moon

Species	Wavelength (Å)	Mercury[a]			Moon[b]	
		g[c] (ph atoms^{-1} s^{-1})	Brightness (R)	N_0 (cm^{-3})	N_0 (Day) (cm^{-3})	N_0 (Night) (cm^{-3})
H	1216	5.3×10^{-3}	70, 720	23, 230[d]	<10	—
He	584	5.1×10^{-5}	70	6.0×10^{3}	2×10^{3}	4×10^{4}
O	1304	2.1×10^{-5}	63	4.4×10^{4}	—	—
Na	5890, 5896	2.45, 1.22	$1\text{-}10\times10^{5}$	$1.7\text{-}3.8\times10^{4}$	—	—
K	7664, 7699	3.24, 1.67	5×10^{3}	5×10^{2}	—	—
Ar[e]	869	5.5×10^{-8}	—	$<6.6\times10^{6}$	1.6×10^{3}	4×10^{4}

[a]Densities or upper limits based on resonance scattering.
[b]Density or upper limits based on *in situ* measurements.
[c]Scattering coefficient (photons atoms^{-1} s^{-1}) at Mercury aphelion and no Doppler shift. For Na and K they vary (see Sec. IV).
[d]Hot and cold components.
[e]Mercurian values inferred from lunar values.

TABLE II
Number Densities at Mercury Terminator: Upper Limits from Mariner 10 Occultation Experiment

	Max. Abundance[a] (10^{15}cm^{-2})	Cross Section (10^{-17}cm^2)	Number Density (10^7cm^{-3})
He	3.7	0.8	2.6
Na	5.0	0.6[b]	11
K	5.0	0.6[c]	14
O	2.5	1.2	4.2
Ar	0.9	3.5	3.1
H_2	2.9	1.0	1.4
O_2	0.9	3.5	2.5
N_2	0.9	3.3	2.3
CO_2	0.4	7.4	1.6
H_2O	0.8	3.6	1.5

[a]Observed upper limit to slant integrated density; value from Broadfoot et al. (1976) except as shown in footnotes b and c.
[b]From cross sections of Samson (1982).
[c]Assumed equal to Na.

atoms and molecules are continually crossing it from below and above. In the exosphere, they are maintained close to a Maxwellian velocity distribution by collisions that occur mainly *below* the exobase.

An important part of our information on Mercury's atmosphere is the distribution of helium over the day side and twilight regions. Lack of agreement with conventional exospheric theory was a major clue that this theory is not applicable. The temperature of the Earth's exobase typically varies by a factor of about 1.3 between day and night, and there is a corresponding excess of H atoms on the night side. This excess can be understood as a balance between a lateral flow of atoms that is more rapid from warm to cold than the reverse. To first order, the density is expected to vary as $T^{-5/2}$, where T is the exospheric temperature (see Sec. V). The observed noon and midnight temperatures on Mercury at aphelion are 575 and 110 K; the ratio of helium densities would therefore be 80. A Monte Carlo simulation of this transport by Smith et al. (1978) gives a ratio of helium densities of 150. This difference is probably due to the inclusion of Jeans escape from the dayside atmosphere in the Monte Carlo calculation. The loss rate by escape is comparable to the flow rate to the night side, and the dayside density is reduced to half what it would be under steady state conditions. The value inferred from Mariner 10 airglow data was 50; the fact that it is lower than both theoretical estimates is probably due to two comparable effects:

1. Helium atoms do not efficiently accommodate their velocity to the temperature of the local surface; indeed, they retain more than 90% of their incident energy after a collision;

2. Interaction of the helium atoms with the surface may not produce velocities sufficient for escape of the atoms.

The physical interaction of the atmosphere with the surface has been treated only in a most rudimentary way in model calculations, and only for sodium and helium. For other elemental species, the only modeling of exospheric distributions has been done with conventional exospheric theory, at least partly because of a lack of physical parameters describing the gas-surface interaction. These interactions are not understood in the required detail (Shemansky and Broadfoot 1977). Relevant properties such as the surface composition and microstructure on Mercury are essentially unknown. The discussion of the surface interactions of atmospheric species on Mercury is limited to known properties of lunar surface material, which is justified only by similarities in the albedo and the general geological appearance. Use of the lunar analogy for Mercury suffers from obvious differences such as proximity to the Sun (temperature) and the presence of an organized magnetic field on Mercury. Perhaps even worse, it is necessary to simplify grossly the surface composition to pure quartz, crystalline SiO_2.

None of the species known to be present in the atmosphere of Mercury can remain bound to the planet for a time comparable to the planet's age, so that there must be a source for each of the elements. Several likely sources of hydrogen and helium have been discussed, but their relative importance is not well defined. The sources of sodium and potassium are even less understood. Several processes may act to remove atoms from the atmosphere, but their relative importance has not been established in all cases. The magnetic field of Mercury may control either the removal or supply of some species to the atmosphere, but the extent and nature of this role have not been established. Examination of Table I reveals remarkable similarities between Mercury and the Moon, for the few comparisons that can be made. We shall examine each of these issues after a discussion of the observations.

II. PRE-MARINER STUDIES

The planning of the Mariner 10 airglow and solar-occultation experiments (UVS, ultraviolet spectrometers) was based on numerous unsuccessful groundbased attempts to detect an atmosphere on Mercury, either spectroscopically or by its scattering of light. This work is now summarized.

The chapter by Dollfus (1961) describes his visual polarimetric measurements at various wavelengths and positions on Mercury's image. Variations with both variables were interpreted as giving evidence for an atmosphere with a surface pressure of about 1 mbar (one millibar is equal to 1000 dynes cm^{-2} or 100 Pa). As he pointed out, it was necessary to assume that the effects were not due to the properties of the surface. This assumption was examined in detail by O'Leary and Rea (1967) who concluded that known

surface effects could indeed explain the results, and suggested that the 1 mbar should be regarded as an upper limit. Further measurements by Ingersoll (1971) extended into the ultraviolet; his photoelectric technique gave no spatial resolution. He found no evidence for gas and reduced the upper limit to a value that depends on composition, but is 0.28 mbar for CO_2.

In a survey of Mercury's atmosphere written for a symposium, Field (1964) considered, along with Dollfus' suggestion, the possibility that an atmosphere might be convecting heat to the night side (then believed to be in permanent darkness). At this time, the 3:2 relationship between orbital and rotational periods and 176-day diurnal period (Pettengill and Dyce 1965) had not yet been established, and there was some evidence that the dark side of Mercury was warmer than expected. Although Field suggested a thin atmosphere, he did not suggest a pressure. In addition to their spectroscopic study, mentioned below, Belton et al. (1967) adapted Field's suggestion to the case of an object with a diurnal cycle. In this version, heat moves vertically through the soil, downwards during the day and upwards at night. The presence of gas can greatly increase the thermal conductivity of a fine powder, and might be revealed by a warmer nighttime temperature. Earth-based measurements available then could not decide the issue. Morrison (1970) presented a thorough review of computations of the thermophysics of the surface, taking into account the varying distance of Mercury from the Sun. The Mariner 10 radiometer (Chase et al. 1976) showed low nightside temperatures that are consistent with a gas-free powder, and fully consistent with the much lower bounds on the pressure set by the UVS.

A number of groups attempted to detect the absorption spectra of common gases, particularly CO_2 and CO; this work is summarized in Table III. Moroz (1965) suggested a marginal detection, which was adopted in a review by Rasool et al. (1965), along with Dollfus' polarimetric argument, as evi-

TABLE III
Spectroscopic Upper Limits for Mercury's Atmosphere

Gas	Wavelength (μm)	Upper Limit (cm-Å)	Upper Limit (μbar)	Authors
CO_2	0.87	not seen		Adams and Dunham (1932)
CO_2	1.6	not seen		Kuiper (1952, p. 352)
CO_2	0.87	5700	4000	Spinard et al. (1965)
CO_2	1.6	~2000[a]	1500	Moroz (1965)
CO	2.35	10	5	Moroz (1965)
CO_2	1.6	200	150	Binder and Cruikshank (1967)
CO_2	1.2	58	40	Bergstralh et al. (1967)
CO_2	1.05	500	360	Belton et al. (1967)
CO_2	2.04	0.2	0.15	Fink et al. (1974)

[a]According to the re-analysis by Belton et al. (1967).

dence for a surface pressure of a few millibars. However, a re-analysis by Belton et al. (1967), with an improved curve of growth consistent with their own new data, showed only an upper limit. With this correction, Table III shows only a sequence of increasingly tight upper limits, the state of knowledge when the Mariner 10 experiments were planned and selected. For a nominal dayside temperature of 500 K, the bounds correspond to number densities of 10^{14} cm^{-3} for CO and 2×10^{12} cm^{-3} for CO_2, far above the Mariner 10 limits in Table II.

The last two columns of Table I give a summary of measurements of the Moon's atmosphere (reviewed by Hodges et al. 1974). Most of the results are from the landed or orbiting mass spectrometers (Hodges et al. 1972; Hodges 1973*b;* Hodges et al. 1973; Hoffman et al. 1973; Hodges and Hoffman 1974), which suffered severe interference during the day from gases emitted by the large quantities of hardware remaining in the vicinity. Attempts to detect H Lyman α were frustrated by the same large interplanetary background that is responsible for the noise level at high altitudes in Fig. 3 below (Sec. III.C) (Fastie et al. 1973).

III. MARINER 10 OBSERVATIONS OF THE ATMOSPHERE

The encounters of Mariner 10 with Mercury took place on 29 March 1974, 21 September 1974 and 16 March 1975. All occurred at aphelion, with the identical hemisphere in sunlight. A good description of encounter geometry, details of events and spacecraft experimental configuration can be found in the book by Dunne and Burgess (1978), and a scientific review is given by Gault et al. (1977).

The Mariner 10 spacecraft included two atmospheric science experiments, the airglow spectrometer and the occultation spectrometer (Broadfoot 1976; Broadfoot et al. 1977*a,b*). The first of these was designed to observe airglow at preselected wavelengths corresponding to the resonance transitions of ionized and neutral helium and of neutral neon, argon, xenon, hydrogen, oxygen and carbon. A separate detector was provided for each line, giving a small spectral window (~20 Å) centered on the resonance wavelength. Two background channels were also provided. Observations during each encounter included scans obtained as the slit was stepped across the planet's visible disk or allowed to drift across it. The second instrument, the occultation spectrometer, used a grating at grazing incidence to obtain simultaneous observations in each of four bands (~75 Å) centered on 470, 740, 810 and 890 Å. These bands lie in the strong ionization continuum of any likely gas, and the four channels were chosen to give rough information on ionization thresholds and therefore identities of any gas detected. The instrument observed the Sun as it was occulted by the limb of the planet. The radiometer experiment (Chase et al. 1976) provided important auxiliary information on the local surface temperature.

A. Resonance Scattering

The intensity I of an airglow emission is conventionally expressed in Rayleighs (R), the photon intensity per steradian multiplied by $4\pi\ 10^{-6}$. Following Chamberlain and Hunten (1987), we write for an optically thin medium

$$4\pi I = 10^{-6} p(\theta) g N \text{ (in Rayleighs)} \quad (1)$$

where $p(\theta)$ is the phase function for single scattering (1 for isotropic scattering, a common approximation), g is an emission rate factor (Table I) in photons atom^{-1} s^{-1}, and N is the line-of-sight abundance in atoms cm^{-2}. The value of g depends on the solar flux at the relevant wavelength and on the oscillator strength of the transition; tables exist for 1 AU (Chamberlain and Hunten 1987; Hunten 1967; Table I). The abundance can be written $N = \eta N_0$, where N_0 is the zenith abundance and η is the airmass factor, equal to the secant of the zenith angle except near the horizontal. For a horizontal line of view tangent to the surface, right through a spherical atmosphere of radius R and scale height H, $\eta = (2\pi R/H)^{1/2}$.

The Mercury-Sun Doppler shift can become large enough to affect the incident solar flux by a large factor. For the alkali metals, this effect is discussed below (Sec. IV). In principle, the influence can be even larger for the ultraviolet resonance lines, but the Mariner 10 encounters all took place near Mercury's aphelion, with a negligible Doppler shift.

B. Helium

Figure 1 shows the brightness observed in the Helium I 584 Å airglow channel during a slow drift across the planet at encounter III, together with the projection of the slit on the disk of the planet during encounter. Also contained in the figure is the result of a model calculation to be discussed below. Figure 2 shows the intensity distribution observed in the same channel during a drift above the bright limb of the planet at encounter I. The observations of helium constitute the best data set for any species observed during the Mariner 10 encounters with Mercury, and their analysis deserves some discussion. The photon flux distribution across the visible disk of the planet can provide directly only column densities averaged over the field of view. To determine the global distribution of helium atoms, one must construct a 3-dimensional model of the atmosphere, combine it with the observational geometry, and predict the observed emission rate. This analysis is necessarily iterative, and must take account of the complications of gas-surface interactions introduced in Sec. I and discussed in Sec. V.

Shown in Fig. 1 as a solid line and in Fig. 2 as a dashed line are the predicted fluxes from Smith et al. (1978) whose work represents the most thorough attempt to treat the helium-surface interaction. The same model was used for both figures. Differences can be seen near the bright limb (Fig. 2), in

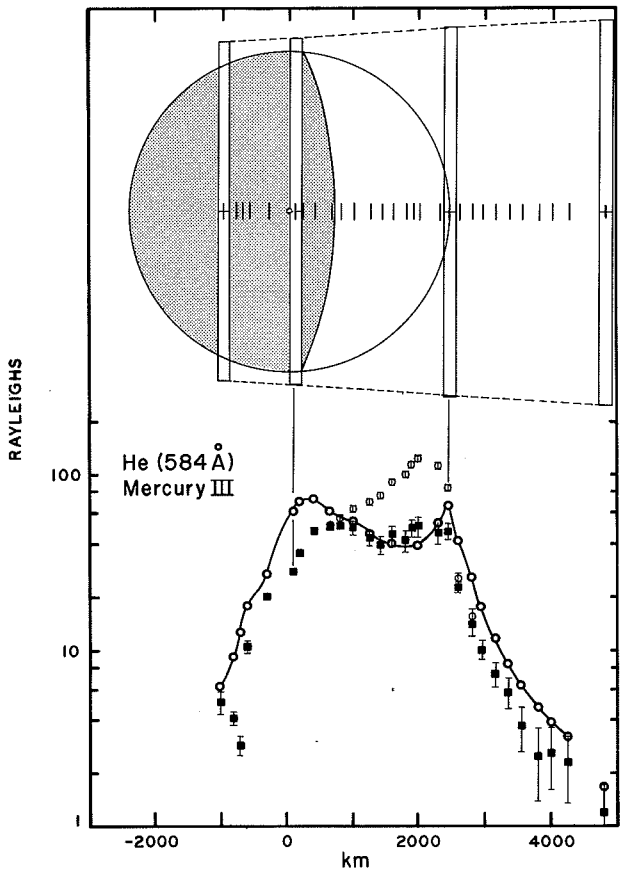

Fig. 1. Mariner 10 ultraviolet spectrometer (UVS) scan of Mercury's disk and subsolar atmosphere, at the helium resonance wavelength. The upper diagram illustrates the projected size of the field of view at four different positions in the scan. Filled symbols have been corrected for planetary albedo, and the open ones are the observed intensities. Circles joined by a curve represent a model described by Smith et al. (1978), which starts with a Maxwell-Boltzmann flux distribution at the surface and includes losses by thermal escape and photoionization. The temperature field is based on Chase et al. (1976) for the evening side of the planet.

the 3000–4000 km region above the bright limb (right side of Fig. 1), and above the dark side of the planet (left side of Fig. 1). Although the model shown represents the best fit that could be obtained, there are significant differences between the model and the observations. The ratio of the number densities at the antisolar and subsolar points is inferred to be ~50. All of these discrepancies make it clear that even the best available model of the gas-surface interaction is still inadequate. More details appear in Sec. V.

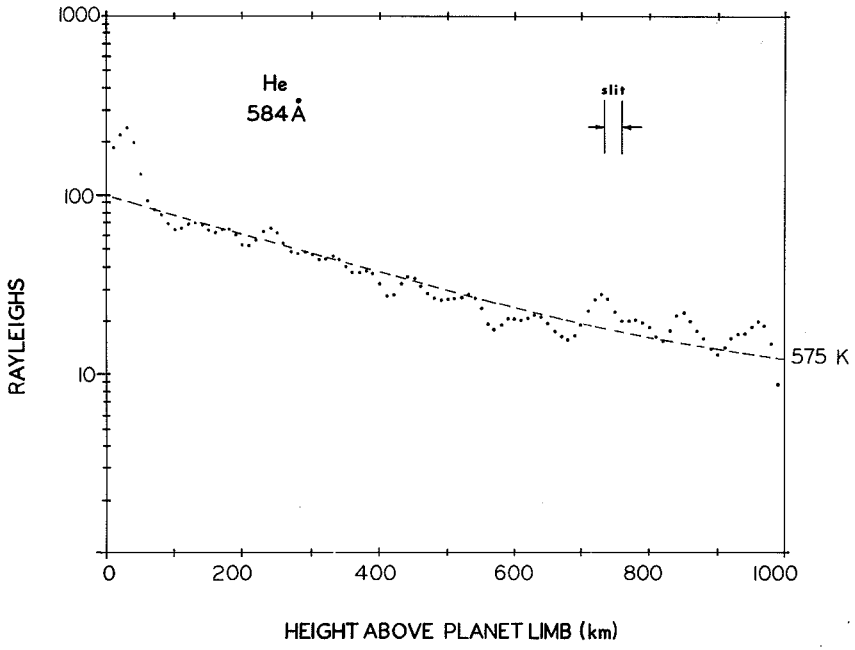

Fig. 2. Close-up scan of the helium distribution above the subsolar limb by the Mariner 10 ultraviolet spectrometer (UVS) (Broadfoot et al. 1976). The projected slit width is also shown. The dashed line is a barometric distribution for 575 K. The bump below 50 km is from planetary albedo.

C. Hydrogen

Figure 3 shows the altitude distribution of the hydrogen 1216 Å emission above the subsolar point determined from encounters I and III. This can be compared with the helium data in Fig. 2. The feature near 200 km is not well understood but may be an artifact unrelated to atomic hydrogen emission. It is not possible to regard this data set as a single population characterized by a single kinetic temperature. Shemansky and Broadfoot (1977) argue that the hydrogen above the subsolar point is in essence a 2-component system consisting of a cold component whose scale height is characteristic of that associated with darkside temperatures, and a second smaller component apparently thermally coupled with the surface near the sub-solar point. The presence of the "cold" population has never been quantitatively explained. Drift scans across the terminator did not lead to a measurable scale height.

D. Oxygen and Other Constituents

The 1304 Å channel detected radiation from oxygen atoms during encounter III. While the signal-to-noise level precluded determination of a scale

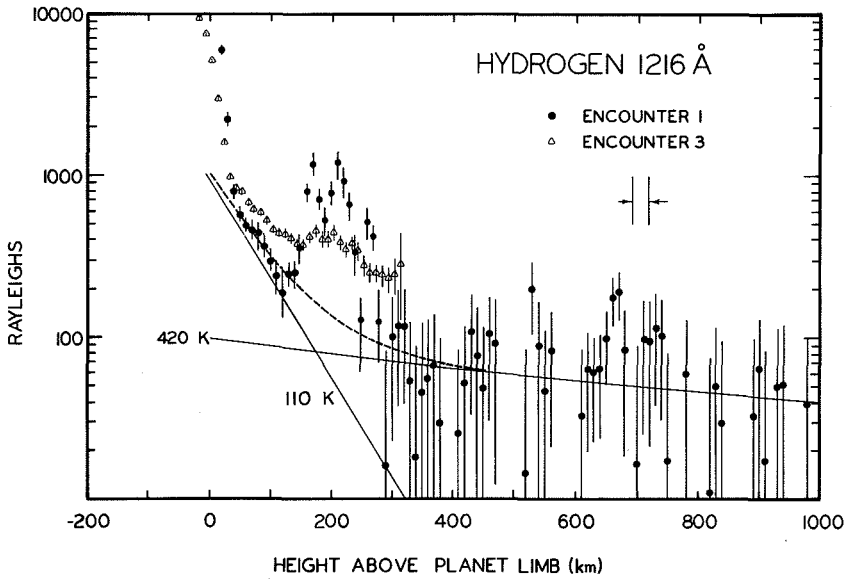

Fig. 3. Same as Fig. 2, but for H in its resonance line, Lyman α. Data from Encounters I and III are included, and a fit to an arbitrary 2-temperature distribution is shown. Information from another scan to higher altitudes contributed to this fit (Shemansky and Broadfoot 1977). Again, planetary albedo appears at the lowest altitudes.

height from the data, it was possible to determine the subsolar point density shown in Table I.

Absorption cross sections are large in the extreme ultraviolet (<1000 Å) for the most likely atmospheric gases, and the Mariner 10 occultation experiment was designed to use these large cross sections to search for the presence of an atmosphere. No measurable absorption was detected in any of the channels. Broadfoot et al. (1976) placed upper limits on common species based on both the occultation and airglow experiments. These are contained in Table II (which includes gases actually detected by the more sensitive resonance scattering method and shown in Table I).

The radio occultation experiment on Mariner 10 (Fjeldbo et al. 1976) also placed an upper limit on the ionospheric electron density, which led the authors to suggest a limit of 10^6 cm^{-3} for the total atmospheric density. This value, which is lower than the results obtained in the EUV occultation, was obtained by analogy with Venus' ionosphere at a similar level. It is not obvious that it would be sustained by a quantitative model of the actual situation at Mercury. Until such a model is worked out, we recommend use of the EUV limits.

Of the undetected gases, by far the most likely to be present is H_2, formed by reaction between implanted H atoms and subsequently released as

further atoms overload the surface grains. (This assertion is controversial; even the present authors cannot agree on it.) As discussed in Sec. VI, a simple scaling from the helium density suggests a dayside value $\sim 10^4$ cm^{-3}, which could be lowered if thermal escape is a more important sink than photoionization. If the maximum estimate is correct, H_2 is almost as abundant as Na. Other hydrides, such as CH_4 and H_2O, should be several orders of magnitude less important. Apart from helium, the most important radiogenic gas is argon, observed on the lunar day side. If the source strengths are similar, and the sinks scale with the solar flux, the dayside density on Mercury might be 300 cm^{-3}.

There is a strong possibility that meteorites are a major source of water vapor, estimated in Sec. VI as having a number density of 2×10^4 cm^{-3}. The lifetime of water vapor is controlled by photodissociation, which in turn is a substantial source of H, H_2 and O.

Hoffman and Hodges (1975) cite evidence for very small amounts of CH_4, NH_3, CO_2, Ne and Ar on the Moon in addition to the established He. CO has not been detected. The rarity or absence of such gases may reflect the absence of a substantial source in the face of the ever-present photoionization sink.

IV. NEW ATMOSPHERIC SPECIES

Sodium D-line emission in the spectrum of Mercury was observed in 1985, and potassium resonance line emission was reported a year later (Potter and Morgan 1985*a*,1986*a*). In each case, the emissions coincided approximately with the bright disk, and the Doppler shifts of the emission lines and the solar spectrum were consistent with the radial velocities of Mercury relative to the Earth and the Sun. Day-to-day variation in the brightness of the sodium emission was noticeable.

Although the discovery is recent, the frequent appearances of Mercury have made it possible to study the spatial extent, to make abundance estimates, and to discuss sources and sinks of sodium and potassium.

The large eccentricity of Mercury's orbit and its rapid orbital motion produce large Doppler shifts, different for reflected solar radiation and resonance emission. The Sun-Mercury component also changes the effective intensity of the exciting radiation, because of the broad, deep Fraunhofer lines due to solar sodium atoms. These and other topics in radiative transfer are discussed next, followed by a description and interpretation of the data.

A. The Motion of Mercury and the Strength of Emission

The solar spectrum incident on an atom of sodium approximately at rest in the Mercurian atmosphere appears Doppler-shifted due to the instantaneous radial velocity of the planet relative to the Sun, v_{rs} in Fig. 4. The effective flux for the resonance transition is therefore modulated. For a shift of zero, the

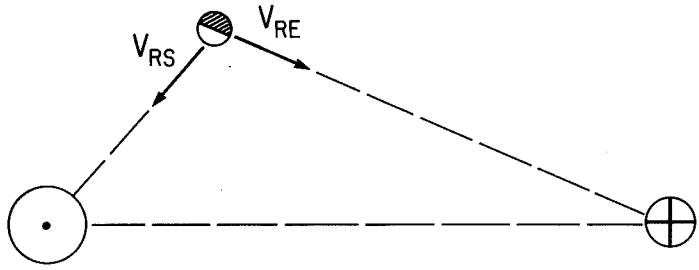

Fig. 4. Illustration of the relevant velocities in the Sun-Mercury-Earth system.

fluxes at D_1 and D_2 are only 5.55 and 4.90% of the nearby continuum. At maximum shift, $\sim$10 km s^{-1}, this fraction rises to 45%. Emission in the rest frame of the planet is observed from the Earth with a Doppler shift v_{re} in Fig. 4. The solar spectrum reflected from the surface is shifted by the sum, $v_{rs} + v_{re}$. Actual data, Figs. 5 and 6, illustrate this. Fig. 5 shows the observed spectrum of Mercury near 5900 Å when v_{rs} was 9.6 km s^{-1} and v_{re} was 34.8 km s^{-1}.

Mercury is a difficult object to observe. In twilight, it appears behind a relatively dark sky, but the time interval in which the planet is visible is short and, because of the large airmass, the seeing is poor and water-vapor lines are strong. In the daytime, the seeing is poor because the Sun is visible, and the sky foreground has a greater surface brightness than Mercury. Spatially resolved spectroscopy has considerable potential for providing information, but is very difficult to achieve in practice. When Mercury is at greatest elongation

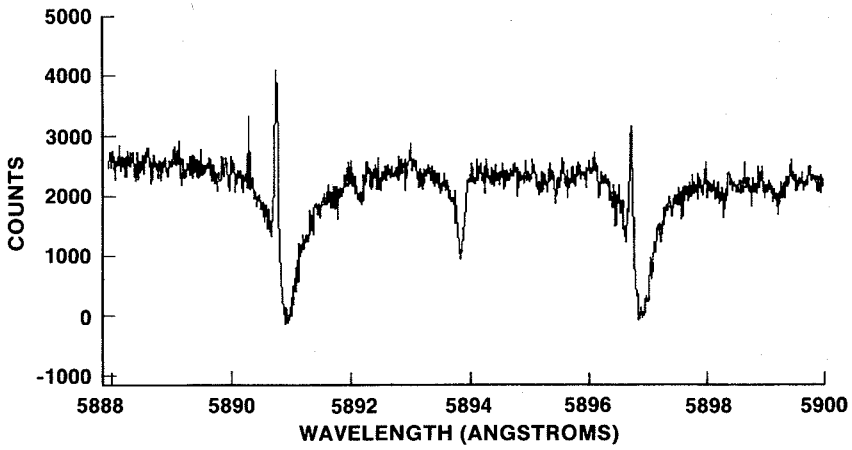

Fig. 5. The discovery spectrum of sodium in Mercury's atmosphere (20:20 UT 3 Jan. 1985) (Potter and Morgan 1985).

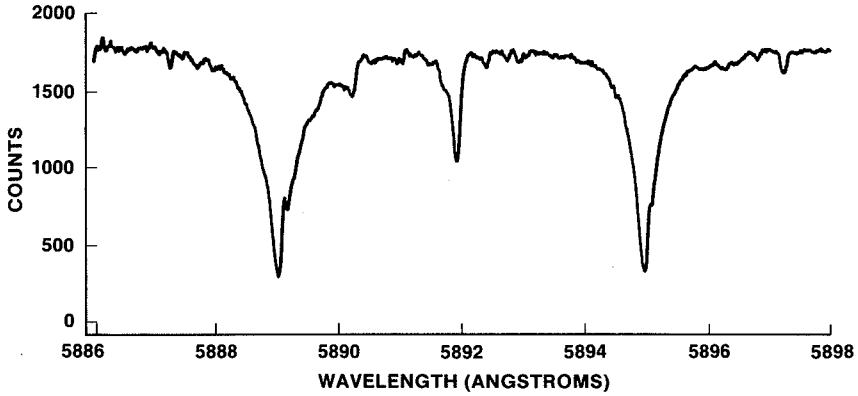

Fig. 6. Another spectrum of the sodium region, showing the Mercurian lines almost hidden in the solar absorptions (16:40 UT 22 Feb. 1986).

from the Sun, its illuminated dimensions are 4–5 by 6–8 arcsec, comparable to a typical seeing disk for the restricted observing conditions.

The observed spectrum is a composite, containing emission from the atmosphere of Mercury, reflected light from the surface, and terrestrial absorption lines due in most cases to H_2O or O_2. Daytime spectra also contain scattered sunlight from the Earth's atmosphere. Terrestrial emission may occur for both sodium and potassium, particularly in twilight, but is not Doppler shifted and thus could not be mistaken for emission from Mercury. The scattered sky component, if present, must be subtracted from the data. The region near the sodium D-lines is relatively free of terrestrial lines, though an H_2O line occurs at 5889.5 Å on the short wavelength side of D_2 and there are many weaker lines. Terrestrial oxygen absorptions partially mask the stronger member of the potassium doublet, but there are frequent occasions when favorable Doppler shifts make observations possible.

B. Physics of Emission in the Sodium D-lines

A large amount of literature exists concerning the sodium layer in the Earth's atmosphere from whose airglow can be obtained temperature, column density and height (Chamberlain 1961; Hunten 1971). More recently, the layer has been studied by lidar, a method that is not applicable to other planets at present. The sodium emissions associated with Io require similar calculations (Chamberlain and Hunten 1987; Brown and Yung 1976). The phenomena are further discussed in Sec. VII. The following brief discussion can be supplemented by the above references and the literature cited in them.

Figure 7 shows an energy-level diagram of the levels that give rise to the sodium D-lines at 5895.92 and 5889.95 Å. The major hyperfine splitting is 21 mÅ. The oscillator strengths are 0.655 for D_2 and 0.327 for D_1. The reported

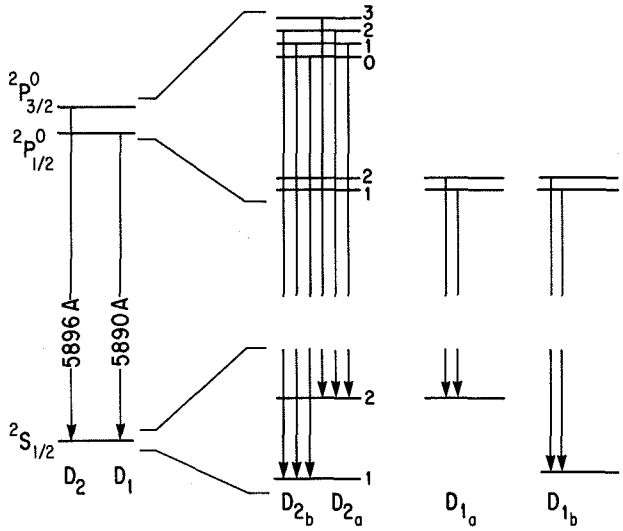

Fig. 7. Energy levels and hyperfine transitions for the sodium D-lines.

measurements of the column density of sodium in the atmosphere of Mercury fall near 10^{11} atoms cm^{-2} and the derived temperature of the gas is at least ~500 K. The optical depth at the center of the D_2 line is ~1: the atmosphere of Mercury is not optically thin and radiative-transfer corrections are required to derive the conditions of the atmosphere from observations. This is particularly true if the data refer to regions near the terminator or limb, for which the incident or emergent radiation has traversed a long slant path. From a knowledge of the wavelengths and oscillator strengths of each hyperfine component, and assumed temperature and abundance, a line profile for each D line is obtained. The path lengths for extinction and scattering are found from the geometry of a particular observation, and the sum gives the monochromatic optical depths for each. For some of the available observations, it has been necessary to average over variable geometry for the areas imaged on the slit. In the case of the sodium resonance doublet, the abundance is usually derived from the ratio of the integrated intensities, which does not require absolute intensity calibration.

At any apparition, a wide range of observing geometries is present across the apparent disk of the planet, and must be considered in interpretation of the results, particularly in estimating abundances. Figure 8 shows the variation of the D_2/D_1 ratio with zenith optical depth for three different geometries. This calculation, which follows Brandt and Chamberlain (1958), assumed a temperature of 500 K, high enough so that hyperfine structure can be ignored to first order. For appreciably lower temperatures, this approximation is not adequate (Chamberlain et al. 1958).

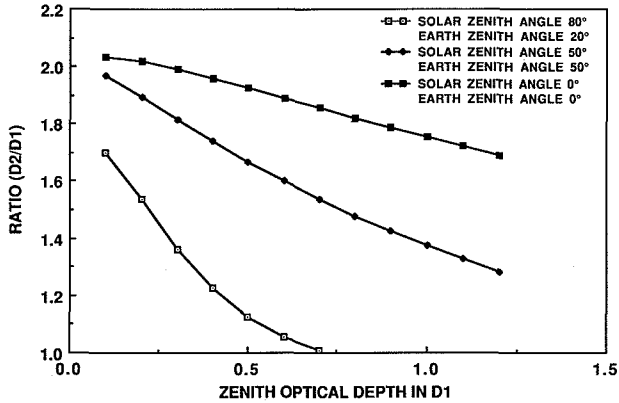

Fig. 8. Sodium D_2/D_1 ratio as a function of zenith abundance, represented by the D_1 optical depth. The three curves represent three different geometries, as indicated.

C. The Density, Physical Extent and Temperature of Sodium

Column densities inferred from the D_2/D_1 ratio range from 1 to 2×10^{11} atoms cm^{-2} (Potter and Morgan 1986*b*). Corrections for hyperfine structure were not included. On average, small values of sodium column density correlate with large solar radial velocities v_{rs}, and large values occur near perihelion and aphelion when the radial velocity is small. Figure 9 is a plot of column density against a measure of the radiation force (Potter and Morgan 1987). Because of the deep Fraunhofer line, radiation pressure effects increase rapidly with radial velocity. Thus, the measurements may reflect increased loss of sodium from the dayside atmosphere when the radiation pressure is large, or perhaps the sodium is being pushed away to the night side, even if it is not escaping. Although this effect is reminiscent of the predictions of Smyth

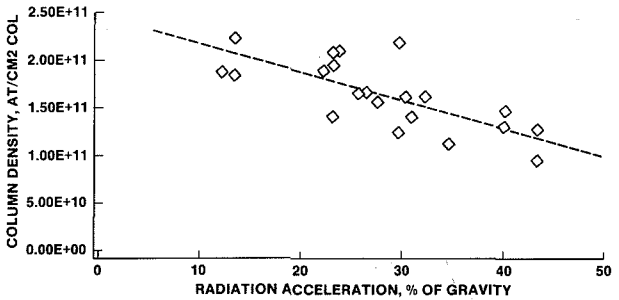

Fig. 9. Sodium abundance as a function of solar radiation pressure (Potter and Morgan 1987).

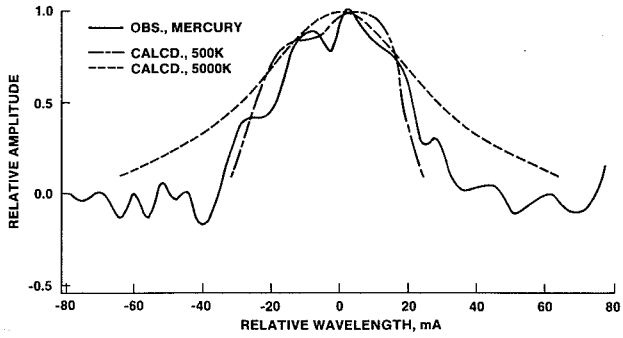

Fig. 10. A partially resolved spectrum of sodium D_2, along with a calculated line for a temperature of 500 K (8 August 1986) (Potter and Morgan 1987).

(1986) and Ip (1986), it probably involves appreciably different conditions. Their models require velocities corresponding to much higher temperatures than are observed, as discussed next (see also Sec. VI).

A high-resolution spectrum of the D_2 line, obtained by Potter and Morgan (1985*b*), is shown in Fig. 10. The 20 mÅ hyperfine splitting is partially resolved, and the FWHM is 55 mÅ, corresponding to a temperature of 500 K, close to that of the surface of the planet included in the slit. At this temperature, the most probable speed is 600 m s^{-1}. In order for radiation pressure to remove sodium effectively, the sodium atoms must have a velocity of at least 2 km s^{-1} (see Smyth [1986] for an in depth discussion). A small population of high-velocity sodium atoms could still be present in the wings of the emission feature, but clearly such atoms are not prevalent. If they are in fact present, but just below the observational limit, losses due to radiation pressure could become significant.

Despite the difficulty of obtaining good spatial resolution, some interesting preliminary observations of sodium are available. Schneider et al. (1985) reported an equator-to-pole variation, and a sunward shift of approximately 1 arcsec in the centroid of the emission relative to the neighboring reflectance spectrum from the planet. They concluded that a genuine separation *might* be present, although different scattering laws for the two spatially distributed sources could also produce the observed shift. Using the same instrumentation and under similar conditions, Tyler et al. (1986) saw no sunward spatial shift, but did confirm the equator-to-pole variation. They also found a north to south ratio greater than unity.

Although Potter and Morgan (1987) were unable to confirm the observations of Schneider et al. or Tyler et al., such differences might be due to differences in viewing geometry. Neither group reports an antisolar tail or any extension of the sodium emission above the dark side of the planet.

D. Physics of Emission in the Potassium Resonance Lines

Potassium and sodium are in the same column of the periodic table, and the spectroscopic terms of the allowed transitions of the two elements are quite similar. However, the potassium lines are optically thin so that a detailed radiative-transfer calculation is not required in order to determine the column densities. The two lines are at 7665 and 7699 Å with oscillator strengths again in the ratio 2:1; because of the large spacing, simultaneous high-resolution observations are difficult to obtain. The stronger line, at 7665 Å, is not usable for Earth airglow studies because it is absorbed by O_2 (see Fig. 11). For Mercury, the Doppler shifts can move it clear of the O_2 absorption where it can be observed.

E. Observations of Potassium

Figure 11 shows the 7665 Å line in the spectrum of Mercury. The average column density on 16 November 1985 was 1×10^9 atoms cm^{-2}, estimated by calibrating the intensity against an assumed intensity in the nearby continuum reflected by Mercury's surface. The sodium abundance was estimated

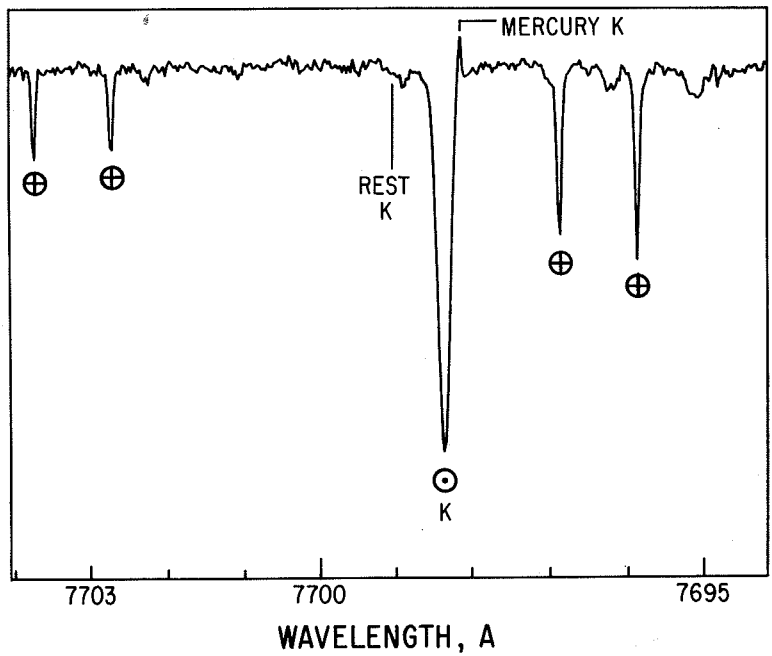

Fig. 11. Mercury spectrum showing the potassium line (8 June 1987, 22:06 UT). The corresponding solar absorption is just to its left, and nearly all the remaining absorptions are by atmospheric O_2. Sky subtraction is almost perfect (figure courtesy of A. Tyler and R. Kozlowski).

from the D_2/D_1 ratio; the sodium-to-potassium ratio, Na/K, is 100. As a comparison, we note that the Na/K ratio for lunar materials ranges from 2 to 7 (Kopal 1974, p. 161), and for the CI chondrites, the Na/K ratio is 13 (Wasson 1985). However, large Na/K ratios can be found in some cometary material. For example, the Na/K ratio observed in Comet Ikeya-Seki was 1000 (Preston 1967), and the VEGA and Giotto measurements of the composition of Comet P-Halley dust grains lead to a Na/K ratio of 188 (Jessberger and Kissel 1987). This probably indicates that similar sink processes are acting to remove potassium and sodium in both the atmosphere of Mercury and in comets that closely approach the Sun, and that the potassium sink is stronger. However, the Na/K ratio on Mercury would also be as it is observed if much of the meteoritic material inside the orbit of Mercury were cometary in origin and deficient in potassium, and if most of the alkalis present in the regolith of Mercury were meteoritic in origin.

V. MODELS OF THE MERCURY ATMOSPHERE

A. Prior Work on He and H and a Comparison of Mercury vs Earth

Previous sections have discussed the available observations of H and He and the conversion of intensities to column densities along the line of sight. Some information about the atmosphere (scale heights, for example) can be retrieved directly from such data, but the iterative process of modeling and comparison must be adopted to extract the full content. If the physical processes that control the atmosphere are well enough understood, this iterated comparison leads to detailed understanding of the atmosphere. Among the most important products which can be derived are inventories for each gas, essential for discussion of sources and sinks.

The atmospheres of the Moon and Mercury are collisionless to a good approximation and thus it was natural to apply the techniques used to study the exospheres of the Earth and other planets. The physics of the terrestrial exosphere is well studied; for example, the distribution of source energies and directions to be used in model calculations is described by the definitive paper of Brinkmann (1971) (cf. Chamberlain and Campbell 1967; Smith et al. 1978). An ideal exosphere, defined by a lower boundary in detailed balance (thermodynamic equilibrium) and a loss-free diffuse upper boundary, contains particles in a Maxwell-Boltzmann kinetic energy distribution (see Feynman et al. 1963; Chamberlain 1963); the ideal exosphere is barometric. Observed exospheres always show deviation to varying degrees from the ideal: escape of light atoms and diurnal variations of exospheric temperature perturb the velocity distribution.

Early research on the exospheres of the Moon and Mercury was thus a direct extension of calculations in which atmospheric particles formed the lower boundary. However, the solid interface at the Moon and Mercury pre-

sented an entirely different problem in the sense that the kinetics of gas particles are controlled by heterogeneous collisions. This fundamental difference was not recognized in much of the early work on the subject. Even the most recent models for the Moon and Mercury contain only rudimentary accounting of the physical interaction at the surface. The physics of gas-surface interaction is crucial for understanding atmospheric evolution on these bodies and must be understood before atmospheric observations can be interpreted in terms of sources, sinks and evolutionary processes. Everything pertaining to the planetary atmosphere depends on the details of the interaction between the gas atom and the surface, along with the competing loss processes.

The following assumptions are implicit in the published models of helium in the atmosphere of Mercury by analogy with a standard exosphere: though there is no net trapping of atoms on the surface, an individual atom that collides with the surface may subsequently have a long (undefined) residence time (chemisorption); and the impact of a helium atom with the surface and the subsequent return of an atom to the atmosphere are independent. Further, it is assumed that the velocity distribution of the atoms returned from the surface is a Maxwell-Boltzmann flux distribution appropriate to the local surface temperature. For a given distribution of surface temperatures, it is then possible to produce a model atmosphere using Monte-Carlo techniques, and from this to calculate a brightness distribution to compare with the data. This class of model was formulated by Hartle (1971) and subsequently used by Hartle et al. (1973,1975*b*), Hodges (1974), Curtis and Hartle (1978) and Hodges (1980*a*). Smith et al. (1978) noted, however, that the interaction of helium, and to a lesser extent any light atom, with the surface under Mercurian conditions is typically a scattering event in which the interaction between the surface lattice and the helium atom is brief and, on average, results in only a small exchange of energy. In short, the interaction of helium with the surface of Mercury violates all of the assumptions given above.

Shemansky and Broadfoot (1977) extended these considerations. The collision of a helium atom with the surface is typically free-free; the consequences include (a) a departure from Maxwell-Boltzmann statistics in the sense that, for a given kinetic temperature, the number of high-velocity atoms is decreased, and (b) a much smaller variation of the surface densities from the subsolar point to the antisolar point than that calculated by Smith et al. Unfortunately, work on the topic was suspended at that point; these ideas have not been pursued to the construction of a model atmosphere of the planet and comparison with the observations. There was, however, some further discussion of the philosophy and methods of computation (Hodges 1980*a,b;* Shemansky 1980).

B. Components of the Atmosphere

The view of the atmosphere taken in this chapter is summarized in Fig. 12. Confusion can easily arise if the distinctions to be discussed are not kept

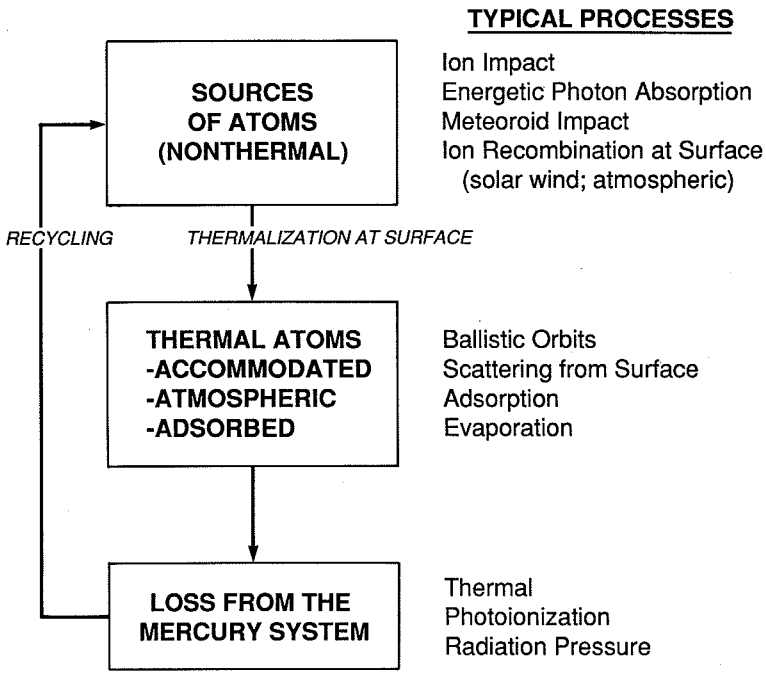

Fig. 12. Processes operating for an atmospheric component.

in mind (Appendix A). *Ambient atoms* consist of atmospheric atoms having energies accommodated to the surface, and their counterparts physically adsorbed on the surface. These two components are in equilibrium with each other; we shall argue that the adsorbed component is by far the smaller, except perhaps for some elements on the night side. *Source atoms* are nearly always more energetic; they are defined as the immediate products of energetic processes such as those shown in the right-hand column. Some may be lost immediately from the atmosphere; the rest lose their energy in impacts with the surface and become ambient atoms.

In this discussion, *sinks* are defined as processes that remove atoms from the planetary environment. Loss processes operate on both source and ambient atoms, but in different proportions. We make the approximation that the sinks operate primarily on the ambient atoms, not on the source atoms, although the proportion undoubtedly depends on the species. Because of the extremely low atmospheric density, any chemical reactions occur on the surface. The mere impact of an atmospheric atom with the surface is not normally considered a sink, because the atom will almost certainly scatter or be thermally evaporated in a very short time. Only if the atom becomes chemically bound to the surface is the impact counted as a loss event for ambient atoms.

A consequence of this view is the existence of two distinct time scales, a longer one for the sources and sinks and a shorter one for interaction of the atmospheric particles with the surface. The latter is the ballistic or free-fall time, which is $\sqrt{2}\ v/g$ for projection at 45° from the horizontal at speed v. Setting v equal to the modal velocity $U = (2kT/m)^{1/2}$, we obtain

$$t_b = \frac{2}{g}\left(\frac{kT}{m}\right)^{1/2} = 2\left(\frac{H}{g}\right)^{1/2} = 52\left(\frac{T}{M}\right)^{1/2} \tag{2}$$

where M is the atomic mass in amu and the temperature T is in Kelvins. Typical dayside values are 250 and 1300 s for thermalized Na and H; a nightside value for Na is 100 s. As a reference for comparison, we may take the shortest well-established loss time, 10,000 s for photoionization of Na; the ratio to the ballistic time t_b is around 40.

Thus, the typical life history of a sodium atom would be: ejection from the surface with energy of a few thousand degrees; several hops with duration decreasing from 1000 to 250 s as the atom thermalizes; ionization after 40 hops. The ion may be lost from the planet, re-implanted in the subsurface, or neutralized at the surface (Sec. VI). Much of the justification for the above statements is given for the atmospheric atoms in the rest of this section, and in the next section for the sources and sinks.

As mentioned in Sec. I, there is a large excess of helium on the cold night side. This excess can be understood as a balance between a lateral flow that is more rapid from warm to cold than the reverse (Hanson and Patterson 1962; McAfee 1967; Hodges and Johnson 1968; Chamberlain and Hunten 1987). To first order, the flow rate scales as $T^{5/2}$, where T is the exobase temperature. To justify this, we consider exospheric atoms to be "hopping" in a random walk from place to place on the exobase and note that the average length of each hop is approximately equal to the scale height. The distance between hemispheres is of the order of the planetary radius r. Since the motion is a random walk, the number of hops is of the order $(r/H)^2 = \lambda^2$ (Eq. 4, Sec. VI), and the migration time is

$$t_m \simeq t_b\lambda^2 = 2gr^2\left(\frac{m}{kT}\right)^{3/2}. \tag{3}$$

For helium at 500 K, this time is 4×10^4 s. The flow rate between hemispheres is proportional to $N/t_m = nH/t_m$, where N is the integrated density. Thus, if a steady state is attained, the product $nT^{5/2}$ should be constant. The H density n on the Earth does vary approximately as $T^{-5/2}$, as expected for "zero net ballistic flow," or ZNBF (Quessette 1972). The surface of Mercury is not a true exobase, but the same tendency should apply there, with other parameters also significant. Quantitatively, the global atmospheric distribution depends on both the kinetic energy distribution imparted by the free-free collision process and the accommodation efficiency of the velocity of H atoms

to the local surface temperature. Nonuniform distributions of sources and sinks are also likely to be significant, especially for the shorter-lived species.

The Monte-Carlo computation for helium by Smith et al. (1978) included the migration process and loss by thermal escape, under the assumption of an accommodated Maxwellian distribution. Without this escape, the result would be expected to follow the $T^{-5/2}$ rule, which gives a night/day ratio of 80. Most of the thermal escape is from the hot day side, and the effect should be to reduce the density there below the steady-state value; the night/day ratio was found to be 150, corresponding to a dayside reduction factor of 0.53. Although it was not explored at the time, this explanation seems reasonable. The $1/e$ escape time (Eq. 7, Sec. VI) would be $\sim 10^5$ s under the assumed conditions; the time to 0.53 is only slightly longer than the migration time of 4×10^4 s obtained above.

As discussed in Sec. V.F below, the migration time for the alkali metals is considerably longer than the ionization time, and the $T^{-5/2}$ rule is unlikely to apply at all.

C. The Gas-Surface Interaction on Mercury

The subject of gas-surface interactions is interdisciplinary, and terms are not always used consistently. Definitions as used here are therefore presented in Appendix A of this chapter. Once again we call attention to the definitions of ambient atoms and source atoms, discussed above and in Fig. 12.

Standard exospheric theory assumes that the downcoming atom is fully accommodated to the exobase temperature and, if ejected back into the exosphere, the initial and final energies are independent. This theory has been applied to Mercury by assuming that the atoms stick to the surface on impact, and the surface simply acts as a saturated source of atoms in a Maxwell-Boltzmann distribution. In reality, most atmospheric atoms are scattered on collision with the surface, and in general there is a relationship between the pre- and post-collision energies of the atom. Physical-scale adsorption collisions on the sunlit surface, when they occur, have durations of only 10^{-13} to 10^{-11} s. The theory of gas-surface interactions is outlined in Appendix B, to supplement the semi-qualitative summary given here. Figure 13 schematically illustrates the potential energy of an atom near a surface. If bound, it vibrates around the potential minimum with average energy kT. For convenience, we express energies E as equivalent temperatures E/k; 1 eV corresponds to 11605 K. Chemical bonds tend to have a strength of a few eV, whereas physical bonds are much smaller, as shown in the second column of Table IV. The observed energy distributions of the atmospheric atoms point to a dominance of physical-scale interaction with the surface even for the chemically active species.

Figure 13 includes a dashed portion representing an *activation energy* E_a. Atomic electron configurations virtually always cause the development of a barrier at intermediate internuclear separations in the collision process. In

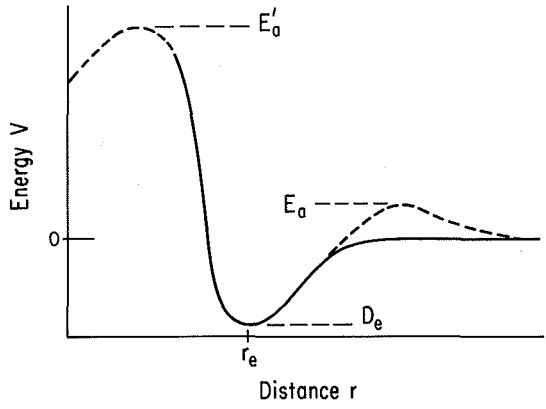

Fig. 13. Schematic potential curve for an atom near a surface. D_e is the well depth, E_a is a possible activation energy, exaggerated for visibility, and E_a' represents an activation energy for diffusion through the lattice.

general, the activation energy is an important factor in limiting the rate of chemical reaction, and sets a lower limit on the kinetic energy of dissociation. For collisions of ground state hydrogen atoms this quantity is very small. However, in collisions of more complex systems including molecular hydrogen, activation energy is a significant rate-determining quantity, and defines the properties of the mutual diffusion coefficient. The interaction terms causing a positive potential at intermediate separations vary in origin from system to system. Finite total electron spin in the interaction (atomic or multiatomic) introduces positive terms in the dispersion energy (see Hirschfelder et al. 1964). Exchange or valence energy terms can also produce positive interaction energies (Buckingham and Dalgarno 1952). It is therefore likely that gas-surface physical interaction also shows positive dispersion energies, but the question is one of magnitude. Hydrogen bimolecular reactions show $E_a \sim D_e/20$, while more complex atomic reactions such as those involving Na show $E_a \sim D_e/10$ (Hirschfelder et al. 1964). For the physical-scale interactions considered here, the value of E_a is expected to be much less than kT, and therefore negligible.

A trapped atom of radiogenic or solar-wind origin is subject to a much larger barrier, indicated in Fig. 13 as E_a'. For lunar material the activation energy for outgassing of helium is ~2 eV (Ducati et al. 1973). Helium diffusing out of the subsurface may then have initial energies of this order.

An atmospheric atom colliding with the surface enters Fig. 13 from the right with energy above zero, corresponding to atmospheric temperature. The atoms will gain or lose energy near the potential barrier in the inner turning-point region, and will be adsorbed only if energy is lost to the lattice structure in sufficient amount to fall below zero. Otherwise the collision will simply scatter the atom.

TABLE IV
Gas-Surface Physical Interaction Parameters for α Quartz[a]

Species	H	He	O	Na	K
Well depth[b] D_e(K)	254	102	920	3000	2800
Well distance[b] r_e (Å)	3.39	2.57	3.11	3.48	4.04
Depth to v = 0[b] D_0(K)	156	54	837	2900	2720
Vibration period $\tau(10^{-13}$s)	2.0	4.7	2.7	1.8	2.5
600 K adsorption time τ_a(s)	2.6×10^{-13}	5.1×10^{-13}	1.3×10^{-12}	2.3×10^{-11}	2.3×10^{-11}
100 K adsorption time τ_a(s)	9.5×10^{-13}	8.1×10^{-13}	1.8×10^{-9}	0.71	0.16
600 K accommodation coefficient α	0.08	0.05	0.11	0.62	0.26

[a]Sources: Kunc and Shemansky (1985) for helium; Shemansky and Kunc (in preparation) for all others.
[b]D_e, r_e, are illustrated in Fig. 13. D_0 is the dissociation energy to the separated-atom limit from the lowest vibrational level.

An adsorbed atom has energy less than zero in Fig. 13, and is oscillating with the vibrational period of order 10^{-13} s. It exchanges vibrational energy with the solid, and after a number of vibrations of order exp (D_0/kT) is likely to have energy D_0 or greater, enough to escape the well (cf. Eq. B1 in the Appendix). If we take Na in Table IV as a specific example, an atom at 600 K in a well with a depth of 0.25 eV, or 2900 K, requires less than 130 vibrations, or 2×10^{-11} s. At 100 K, these values rise to 4×10^{12} and 0.7 s. Since the ballistic times are 100 s or greater, fewer than 1% of sodium atoms are expected to be adsorbed to the surface, even on the night side; for other observed atoms this fraction is much smaller still. For the much hotter subsolar surface, it appears safe to conclude that the majority of collisions do not involve adsorption for any of the known atmospheric gases, and that the few that do adsorb are rapidly re-emitted.

Along with these very short interaction times goes a strong possibility that the speed distribution of the atmospheric atoms is non-Maxwellian. There are extra drains on the faster atoms: they may be able to escape, and even the gravitationally bound ones are exposed for longer times to loss processes such as photoionization. Restoration of the high-energy tail must therefore occur during interactions with the surface, which appear to be very inefficient. The only detailed information available is for helium, but the same ideas can be expected to apply to the other light atoms and especially to H.

Shemansky and Broadfoot (1977) report the result of a calculation of the He 1-dimensional energy distribution in equilibrium with a surface of SiO_2 (Fig. 14). A Maxwellian distribution is shown for comparison, and the deviations are obvious, especially at high energies. This calculation, described in Appendix C, is intended to give a statistical equilibrium between the gas atoms and the surface. It appears that the energy transfer in a single collision is limited to the maximum phonon energy. (A phonon is a quantum of the lattice vibrations in a solid; the typical energy corresponds to the Debye characteristic temperature.) If the system were a closed, isothermal cavity in thermodynamic equilibrium, the velocity distribution would approach a Maxwellian after a large number of collisions (including, of course, rare collisions among atoms). However, Mercury's atmosphere is very different: the surface itself is not in thermodynamic equilibrium, and the approach of the atmosphere to a steady state must take into account competing processes. The need for replenishment of high-speed atoms has already been mentioned; moreover, the planet is very far from isothermal. Further work is required.

The same computations give an *accommodation coefficient* α for helium, shown in Table IV as 5% (Shemansky and Broadfoot 1977; Kunc and Shemansky 1985). As defined in Appendix A, α is an efficiency for energy transfer in a collision with the surface. However, this quantity alone, determined by a classical calculation, cannot define the energy distribution function in the gas because it contains no information about energy dependence.

The principal characteristics of surface reactions with light atoms have

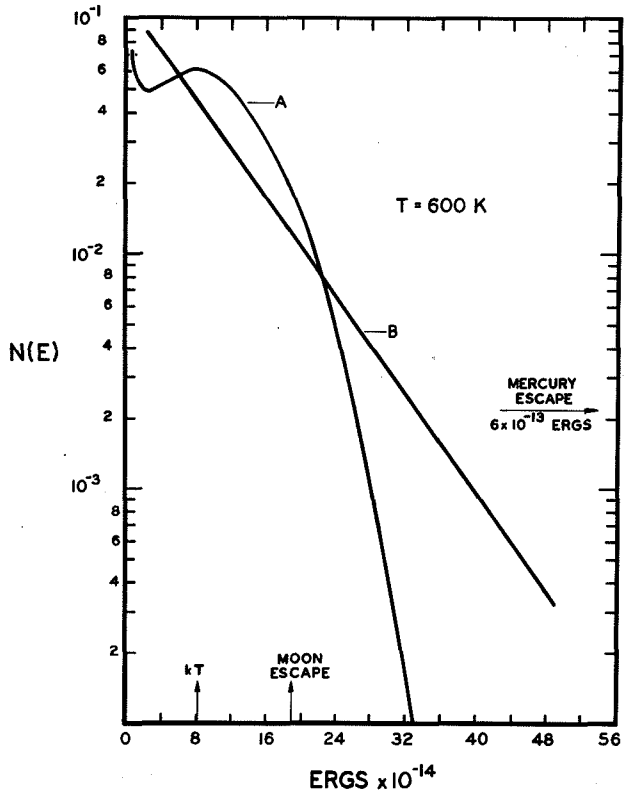

Fig. 14. Calculated one-dimensional energy distribution for helium atoms interacting with a surface of SiO_2 at 600 K (curve A). Curve B is a thermal distribution for the same temperature (Shemansky and Broadfoot 1977).

been summarized by Shemansky (1980). The two effects mentioned above as controlling factors in the global atmospheric distribution of gas are closely coupled physically: a low accommodation coefficient is accompanied by a truncated energy distribution. The reason is that energy exchange reactions are limited to single phonons, defined by the Debye characteristic temperature of the solid. A low accommodation coefficient implies rapid transport of gas, because successive hops along the surface are strongly coupled in direction as well as speed. Thus, the effective mean free path along the surface may be greatly increased. This high mobility must, however, be reduced by microscopic surface roughness and by the inherent angular scattering distribution. Another effect, which decreases mobility, is a small reduction in the mean energy of the gas below that calculated from the surface temperature because of the truncated energy distribution. Although these effects are in opposition, it seems likely that the net effect is an increased mobility. The magnitudes

probably depend on the parameters of the particular gas. Heavier atoms are expected to approach a Maxwellian distribution in statistical equilibrium more closely because multiple-phonon exchanges are more probable (see Table IV). Moreover, the processes (such as escape of the faster atoms) forcing the distribution away from being thermal are weaker.

Gas-surface interaction theory generally assumes that the dominant energy exchange involves the surface normal component of the velocity vector of the gas atom. The quality of the surface consequently plays a role in determining both the effective accommodation coefficient and the angular scattering distribution, and hence the transport properties.

D. Helium

The enhanced transport rate discussed in the previous section presumably explains the discrepancy between observation and earlier model calculations that implicitly assumed an accommodation coefficient $\alpha = 1.0$. The truncation of the tail of the energy distribution is predicted to reduce greatly the thermal escape rate of helium from the subsolar atmosphere in comparison with that expected for a gas in thermodynamic equilibrium at the surface temperature. The theory of gas-surface interaction thus directly affects ideas on atmospheric evolution. Similar considerations have yet to be applied to the other atmospheric gases, and will have to recognize that almost every physical aspect depends on the species.

All atmospheric model calculations published to date are limited by the assumption of thermodynamic equilibrium at the surface. Calculations by Hartle et al. (1973,1975*b*), Hodges (1974) and Curtis and Hartle (1978), all follow essentially the same computational method, whose properties and limitations have been discussed above. All of these papers generate their velocity distributions by a method intended to simulate an atmospheric gas in thermodynamic equilibrium at the altitude of the surface, and at the local surface temperature. However, Smith et al. (1978) show that the previous calculations contain an inadvertent mix of two different source distributions, giving a nonbarometric atmosphere under idealized conditions. They presented results of a Monte Carlo calculation using a source flux correctly formulated for a gas in thermodynamic equilibrium. The temperature distribution used was that measured by Chase et al. (1976). The night/day density ratio for helium at the antisolar and subsolar point was found to be ~150 (see also Sec.V.B above). A separate calculation based on the analytic formulation of Hodges (1973*a*) produces essentially the same result (Smith et al. 1978).

The comparison of model and data (Fig. 1; Broadfoot et al. 1976; Smith et al. 1978) indicates a night/day ratio ~50. This discrepancy is the basis for the statement made repeatedly above that a theory based on a fully accommodated gas-surface interaction does not account for the observations. The required large mobility across the surface may be consistent with the He accommodation coefficient for a single scattering event. Table IV shows $\alpha = 0.05$

for alpha-quartz and it is expected to be similar for many other inorganic surfaces (Shemansky and Broadfoot 1977); this value may be small enough to explain the data. However, the translation of a mean accommodation coefficient into an atmospheric distribution is not a simple matter. The classically calculated accommodation coefficient is a single number, and does not provide the necessary probability distribution for energy exchange. Without this, it is not possible to calculate distribution functions for kinetic energy and direction, which affect mobility, height distribution and the rate of thermal escape. The angular distribution of the scattered atom depends both on the detail of the energy exchange process and the quality of the surface (Shemansky and Broadfoot 1977).

The night/day ratio is also affected by asymmetry in the loss process. In the calculations of Smith et al. (1978), Jeans escape was the major sink, whereas, in fact, photoionization probably dominates, with a different distribution and a considerably smaller rate. However, it too acts primarily on the day side and should also act to somewhat increase the night/day ratio.

Table V shows the estimated global content of helium based on Mariner 10 observations, and with the assumption of a nightside density enhancement of 50; it corresponds to the number quoted by Goldstein et al. (1981).

E. Hydrogen

Figure 3 illustrates the distribution of H Lyman α radiation above the subsolar surface, already described in Sec.III.B. There are unexplained features, specifically the presence of two components and their small scale heights (Shemansky and Broadfoot 1977) (see Sec.III.C). (The bump in encounters I and III near 200 km is a complete mystery.) One component appears to have a temperature (420 K) 40% below the local surface temperature. This component is best seen in high-altitude data, not reproduced here, obtained from a greater distance (Broadfoot et al. 1976). Even if the disagreement is outside the errors, it may be that the appropriate surface temperature is a dayside average rather than the local value. The dominant population in the subsolar atmosphere is very cold (100–150 K; Fig. 3). The H abundance of the cold component is ~50% larger than that of the warm component. The obvious source for cold atoms is the dark side, but such atoms would have to survive a large number of collisions with warmer surfaces without gaining energy. Hydrogen probably does have a higher mobility than helium, even though the accommodation coefficient (α = 0.08, Table IV) may be larger. Perhaps further study will show that the nightside source is viable.

Broadfoot et al. (1976) suggested that the small scale height reflects that of a source gas, namely H_2O, the H atoms being produced by photolysis. As discussed below in Sec. VI, this process seems to require an unreasonably large amount of water vapor.

Alternately, one could consider interactions with the local surface along with selective thermal escape of the faster atoms. Mercury's escape velocity is

TABLE V
Estimated Atmospheric Physical Properties on Mercury

	H	He	O	Na	K	Notes
SCALE HEIGHTS (km)						
Subsolar H_s	1330	330	83	58	33	a
Antisolar, H_a	230	57	14	10	6	b
Dayside content (10^{27} atoms) N_d	4	100	140	60	0.7	c
Nightside content (10^{27} atoms) N_n	4	670	2200	60	0.7	c
PHOTOIONIZATION TIME (s)	5.5×10^6	3.8×10^6	8.8×10^5	12,800	7500	d
PRODUCTION RATES, (10^{22} s^{-1})						
Radiogenic, P_r	—	0.7–4.6	—	—	—	e
Sputtering, P_{sp}	—	—	30–300	3–30	<1	f
Photosputtering, $P_{\phi s}$	—	—	?	10;<2000		f,g
Meteoritic, P_m	—	—	—	2–14	0.3	h
Interplanetary medium, P_{ipm}	1.4	0.2	—	—	—	e,o
Solar wind + magnetosphere, P_{sw}	230–850	10–37	—	—	—	e,i
LOSS RATES, (10^{22} s^{-1})						
Jeans	<<80	—	—	—	—	j
Photoionization	<0.14	<13	<50	≤600	≤10	k
Solar-wind, magnetosphere ionization	0.09	0.06	1.3	0.04	.0008	l
Radiation pressure, nonthermal atoms				?		m
ATMOSPHERIC LIFETIME (hr)	$(8–70)\times10^3$	$(7–70)\times10^3$	>7000.	>5.	>3.	n

a: T = 575 K; b: T = 100 K; c: From Table I and above scale heights. Area of a hemisphere = 3.75×10^{17} cm^2. Night/day density ratio taken as 1 for H, 50 for He, 100 for O, and 1 for Na, K; d: Kumar (1976) and Sec. VI; e: Goldstein et al. (1981); f: Ip (1986); g: McGrath et al. (1986); h: Sec. VI; Morgan et al. (1987); i: H value assumed to be 23 times He; j: Sec. VI; k: Upper limits assume no recycling of ions from magnetosphere to surface; l: He value from (e); others are probably comparable if scaled by abundances; m: Smyth (1986); Ip (1986); n: Ratio of estimated content to loss rate. It does not include possible losses of source atoms. o: Assumed deposition efficiency 0.3.

4.25 km s^{-1}, and the modal velocity U, defined above, see Eq. (2), is 3 km s^{-1} at 600 K. Almost the entire upper half of the Maxwellian distribution must be essentially missing, and surface collisions are very inefficient at repopulating it. It seems unlikely that the resulting distribution would resemble that for 100 K, but in the absence of any computations there is no point in speculation. The global content of atomic hydrogen is poorly defined because the strange distribution observed above the subsolar surface is not well understood, and measurements are not available elsewhere on either hemisphere.

The calculated subsolar scale height H_s = 1330 km for atomic hydrogen shown in Table V is ~40% larger than the measured value, as mentioned above. The global content given in Table V ($M = 8 \times 10^{27}$ atoms) is estimated by assuming the same amount on night and day sides. This assumption is justified by the presence of the cold component in the subsolar H distribution and the further assumption that this cold gas has been transported from the dark hemisphere.

F. Sodium and Potassium

The physical interaction potential D_0 for the Na-quartz system calculated by Shemansky and Kunc (1987) is estimated to be ~3000 K or ~0.26 eV in depth (Table IV). The accommodation coefficient is large (~0.6); thermalization at the surface is efficient, in accord with the observed line width. Model calculations attempting to define source and atmospheric distribution have been published by Ip (1986), Smyth (1986) and McGrath et al. (1986), and are also discussed in the next section. There has been a tendency to assume that the sodium is hot and occupies a very extended height region, but the evidence does not support this idea. The velocity distribution appears to correspond to the surface temperature (Fig. 10), and only a few bounces from the surface should be sufficient to approach this condition. The scale height at 600 K is only 60 km. Nevertheless, Fig. 10 could not be used to refute (or support) the presence of a sodium component with a temperature of several thousand degrees and comparable area, but 2 to 3 times the width and 1/2 to 1/3 the height.

Radiation pressure exerts a strong antisunward force, especially when the Mercury-Sun Doppler shift is large, and is integral to the models of Ip and of Smyth. Such transport may be effectively dampened by efficient thermalization at the surface and the short photoionization time. Observations of the behavior of sodium throughout the Mercurian year, such as those in Fig. 9, promise to shed light on this issue.

The discussion by McGrath et al. (1986) does not clearly distinguish between source and ambient atoms, but the lifetime they adopt pertains to the latter. They conclude that the principal source (of atmospheric atoms) is "thermal desorption," or evaporation. To this we would add that only a very small fraction of the free sodium is adsorbed to the surface, and that the majority of the impacting atoms are most simply regarded as scattering, rather than con-

densing and then evaporating. In this connection, it is interesting to look at the volatility of sodium metal, simply as a rough indication of what to expect at Mercury. A typical dayside density of 3×10^4 cm^{-3} would be attained at a temperature of around 290 K, a rather cool room temperature. Much smaller densities would, however, be expected in the 100 K range, to the extent that such an analogy is applicable.

Under steady state conditions, an ambient, thermal atmosphere with a relatively large accommodation coefficient should have most of its atmospheric content in the unobserved dark hemisphere. This situation probably does not exist for sodium and potassium. The migration time for Na, estimated from Eq. (3), is $\sim 10^6$ s, far longer than the photoionization time, and only an order of magnitude shorter than the 88-day alternation of day and night. Radiation pressure, suggested as the explanation of Fig. 9, may produce some nightside enhancement, but it is probably small. The entry for the nightside content in Table V therefore does not include any enhancement. If the principal source is global, there could be a large nightside enhancement.

Although this discussion is phrased in terms of sodium, much of it pertains equally to potassium, given how much less is known about its atomic physics and its behavior on Mercury. Relevant figures are given in Tables IV and V.

VI. SOURCES AND SINKS

The "ambient atoms" in the central box of Fig. 12 have been discussed in Sec. V; this section concentrates on the upper and lower boxes, the generation of source atoms and the loss of ambient atoms. The possible sources discussed in the literature are capture and neutralization of solar-wind ions, impact of atoms from the interstellar medium, sputtering of surface material by impact of energetic ions or photons and vaporization by meteoroid impact. For helium (and argon, detected only on the Moon), degassing of radiogenic atoms is another possibility, although Ducati et al. (1973) suggest that this source is small compared with the solar wind. Although some source atoms probably have energies in the thermal range, it seems likely that most have higher energies, and extend to correspondingly greater heights. Ejection of chemically bound atoms, with binding energy of a few eV, is likely to give velocities higher than thermal, especially in photo-ejection or sputtering by a photon or an ion with excess energy. Moreover, if an atom must overcome an activation energy E_a to be released, it should have kinetic energy equal to at least E_a. The absence of such energies in the data of Fig. 10 does not rule out the presence of energetic atoms, but suggests that they are less than half the total population, at least for sodium.

The rate at which any of the atmospheric species is replenished to make up for loss is difficult to define with a satisfactory degree of accuracy. Observationally, the source particles appear to be masked by an ambient pool of gas; observed mean kinetic energies are at or below the surface temperature. As

argued in the previous section, the residence time of an atom must be several times longer than the characteristic time for accommodation with the surface.

Thermal escape is probably the most important loss process for H, and perhaps also He, but these rates are not readily calculated because the velocity distributions are highly non-Maxwellian. (Escape from the Moon is likely to be thermal for both H and He.) For the other gases, as well as He, the lifetimes are probably limited by photoionization. Radiation pressure affects the escape rate of source atoms of Na and K, but the ambient atoms are much less affected. The rates of photoionization are reasonably well defined for all of the species, but the efficiencies with which the ions are lost from the system are very uncertain. Table V gives rough estimated quantities for the known atmospheric species.

The next two subsections discuss general characteristics of sinks and sources; sinks are treated first because the rates are easier to estimate. These concepts are then applied to the individual groups of atoms.

A. Sinks and Lifetimes

Thermal Escape. As mentioned above, light gases should escape rapidly from a planet as small and as hot as Mercury if their energy distribution is Maxwellian. Thermal escape is conveniently discussed in terms of the dimensionless parameter

$$\lambda = r/H(r) \tag{4}$$

where the scale height is

$$H(r) = \frac{kT}{mg(r)} = \frac{kTr^2}{mg_0} \tag{5}$$

where r is the planet-centered radial distance, $H(r)$ is the atmospheric scale height, and g_0 is gravitational acceleration at r_0, the radius of the solid planet. Small values of λ_0 imply very rapid escape from the planet's surface; the time scale can be obtained by taking the ratio of the integrated density $n_0 H(r_0)$ to the Jeans escape flux:

$$\tau_J = \frac{2\sqrt{\pi}H(r_0)\exp(\lambda_0)}{BU(1+\lambda_0)} . \tag{6}$$

As before, U is the most probable thermal velocity. The quantity B multiplies the flux obtained for a pure Maxwell-Boltzmann distribution to correct for a reduced population at high energies (Brinkmann 1971; Shizgal and Blackmore 1986). It is usually 0.5 or greater for a standard exosphere, but is expected to be much smaller for Mercury and the Moon. To obtain a crude idea of the lifetime, we can take values (except in the exponential) appropriate

for helium on the day side of Mercury: $H \sim 300$ km, $\lambda_0 \sim 10$, $U \sim 1$ km s^{-1}; the lifetime in seconds (Eq. 6) becomes roughly

$$\tau_J \sim \frac{100}{B} \exp \lambda_0 \tag{7}$$

With $\lambda_0 = 5$ to 10 and B not much smaller than unity, we obtain extremely short times of 15000 and 2×10^6 s. Since B is almost certainly very small for H and He, Eq. (7) actually gives only an extreme lower bound. For atomic oxygen, λ_0 is around 40, for which this lifetime approaches the age of the solar system.

As Fig. 14 shows, collisions of helium atoms with a quartz surface are very inefficient at populating the higher energies, and a similar statement can be surmised to hold for H. Simultaneously, the escape process is strongly draining the same energies. As the escape velocity is around 1.4 U for H at subsolar temperatures, and 2.8 U for He, the effect on the escape rate and the velocity distribution is certainly large. Just how large will not be known until a self-consistent numerical calculation has been carried out.

Radiation Pressure. The acceleration of an atom of mass m due to resonance scattering of solar radiation is

$$a_n = (\pi h e^2 \nu_i / m_e m c^2)\ (\pi F_{\nu_i})\ (f_i / R^2) \tag{8}$$

where e, m_e are the charge and mass of the electron, ν_i and f_i are the frequency and oscillator strength of the resonance transition, πF_ν is the solar flux at 1 AU (in photons cm^{-2}s^{-1}) in the rest frame of the atom, and R is the distance from the Sun in AU.

The solar flux at the resonance wavelengths of Na and K not only excites the observed scattered light, but is also strong enough to produce significant accelerations of the atoms. (For H, the acceleration is roughly equal to that of solar gravity, ~ 4 cm s^{-2}, but still much smaller than that of a planet.) The presence of a deep Fraunhofer line affects the radiation pressure in exactly the same way as the resonance scattering; Doppler shifts relative to the Sun can increase the acceleration by an order of magnitude or more (Smyth *1986b*). For sodium, taking into account both fine-structure components, the acceleration can reach 200 cm s^{-2}. In a single dayside hop of 250 s, the increment of velocity is as great as 500 m s^{-1}. The value for potassium is always larger, because the Fraunhofer lines are neither as deep nor as wide, even though the continuum flux is less by a factor of 2/3.

The relevant radial velocity includes the motion of the atom relative to that of the planet, which changes as the atom is accelerated; it is therefore necessary to follow the motion with a computer. Such computations have been carried out by Ip (1986) and Smyth (1986) for Na. The effect on the escape

rate is minor unless the ejection velocity from the surface is at least 2 km s^{-1} (3 km s^{-1} if the Mercury-Sun radial velocity is small). To obtain appreciable populations at these velocities from a thermal distribution would require temperatures of 1000 to 2000 K for sodium. Compared with the example in the previous paragraph, such velocities allow a longer time for the acceleration to operate, and also a reduced planetary gravity. Under such conditions, a comet-like tail is predicted and the loss rate from the planet is enhanced. The effect is larger if the planet is already moving away from the Sun. If the planet's motion is towards the Sun, the atom moving in the opposite direction sees the weaker radiation near Fraunhofer line center and is accelerated less.

The importance of radiation pressure as a loss mechanism for the alkalis therefore depends crucially on whether there is a substantial population of nonthermal atoms in the atmosphere, that is, source atoms that have not been thermalized by collision with the surface. According to Table IV, the accommodation coefficients are large for the alkali metals, and most of the atmosphere should be thermalized. This conclusion accords with the observed D_2 line profile (Fig. 10), although a substantial component at a few thousand degrees cannot be ruled out in the absence of data with a higher signal-to-noise ratio.

Since radiation pressure requires a substantial time to build up a significant velocity, the competition by photoionization as a loss mechanism must be considered. For illustration, with the maximum acceleration of 200 cm s^{-2}, the time required to build up a speed equal to the escape velocity (4.25 km s^{-1}) is 2100 s, not much less than the ionization time of 6000 to 12,000 s.

Ionization. Photoionization times are short, especially for the alkali metals (Table V) where the lifetime in daylight is around 3 hr (half as great at perihelion). Whether the ion is lost from the planet depends entirely on the characteristics of the magnetosphere and solar wind environment. If the magnetic field were an undisturbed dipole, the ion would rise or fall at the same rate as its parent atom, being simply constrained to spiral along a field line until it would hit the surface and be neutralized. However, the actual field is rapidly convecting, its outer parts driven downstream by the solar wind; an equivalent picture is that there are large electric forces on the ions, much larger than gravity. Although many of the ions are therefore swept away in the solar wind, some fraction are aimed back to the surface, particularly at high latitudes or on the night side, where they can be neutralized and re-emitted. Goldstein et al. (1981) discussed these processes and settled on an escape fraction β of 0.5 for He, with a range from 0.25 to 1; Ip (1986) prefers 0.8 or 0.9. On grounds similar to those discussed below, McGrath et al. (1986) suggest $\beta \sim 0.1$ for Na, which is low enough to have a significant effect on sodium budget assessments.

Thermal alkali atoms, in particular, are confined within 100 to 200 km of the surface, and ions produced there may be at least partially protected from

magnetospheric sweeping. Such protection could be very important if the surface were a conductor, which it almost certainly is not. Possible effects are the presence of a weak ionosphere and a small inward component of the electric field which would carry ions into the surface. Such effects need quantitative assessment; at present we can only guess that they will lower the escape fraction and adopt the 0.1 of McGrath et al. Thus, for sodium near aphelion, an average atom would be ionized every 10^4 s and would be recycled 10 times before escaping from the planet, for a total lifetime of 10^5 s, just over an Earth day. The sodium budget, discussed below, suggests that a still smaller escape fraction may be required.

B. Sources

Atmospheric H and He would seem likely to arise from neutralized solar-wind ions, and O, Na and K from meteorites or from Mercury's crust and interior. However, helium could be degassed from the interior, as on the Earth, although Ducati et al. (1973) conclude that atoms from this source are negligible in the gases trapped in lunar grains. The elements discovered by Mariner 10 were discussed by Kumar (1976), and capture and loss processes involving the solar wind by Banks et al. (1970) and Goldstein et al. (1981). Since the discovery of the sodium atmosphere, papers have been published by Ip (1986), Smyth (1986) and McGrath et al. (1986).

Capture of Solar Wind. Mercury's magnetic field is just strong enough to deflect the solar wind away from the surface under average conditions, but not all of the time (Chapter by Russell et al.; Goldstein et al. 1981). Rapid magnetospheric convection is probably accompanied by entrainment of solar-wind ions, many of which are precipitated to the planet in the same way as auroral ions on Earth. The ions impinging on the surface are probably implanted initially. They must be released in some separate process, which may be thermal or involve displacement by another newly arrived ion. These processes have been surveyed in detail by Goldstein et al. (1981), who give many references to earlier literature. They conclude that a fraction between half and all of the implanted gas is eventually released. Formation of H_2 seems likely to be the fate of much of the hydrogen, but theoretical arguments to the contrary have been suggested. Such arguments tend to be based on the notion of small quantities of H trapped at isolated sites in a nearly ideal crystal lattice, hardly applicable to the lunar surface nor that of Mercury. In addition, the probable rarity of H atoms trapped in soil grains (cf. Ducati et al 1973) may suggest that they are unlikely to encounter one another. We find below that there is a severe deficiency of atomic H on both bodies, and formation of molecules is by far the most likely explanation.

The results of the study by Goldstein et al. (1981) are summarized in Table V. Further discussion appears below in Sec.VI.C. They find that the solar wind has direct access to the surface of Mercury only ~6% of the time;

this access is supplemented by indirect magnetospheric processes. It is possible that this estimate may be too low: the UV albedo of Mercury is lower than that of the Moon (Wu and Broadfoot 1977), and a decreased albedo is a characteristic of proton irradiation (as opposed to α particles: Zeller et al. 1966). According to the latter authors, chemical reactions in the solid are most efficiently produced by protons having energies of 5 to 20 eV.

Retention and diffusion of gases in lunar glasses (the major component of the regolith) have been thoroughly discussed by Ducati et al. (1973). Helium is retained much more tightly than in synthetic glass of similar composition; they suggest that the structure is altered by the irradiation received on the Moon. Both He and Ne are released in the range between 900 and 1300 K, corresponding to an activation energy for diffusion of around 2 eV. The incident solar wind should be able to saturate the surface, to levels of 10^{17} and 10^{16} cm^{-2} for H and He, in 10 yr. The amounts observed are lower by 2 orders of magnitude. As another indication, the He/Ne ratio is ~50 instead of 600 in the solar wind, and the neon itself is reduced by a factor ~50 relative to nitrogen. It is clear that, for atmospheric purposes, hydrogen and helium are not retained in the solid. The H density may even remain so low that H_2 formation is inefficient. If H atoms are released with nonthermal energies, they would be rapidly lost from the planet. In addition their very large scale height would make them difficult to detect, because they could not easily be distinguished from the background of the interplanetary medium.

Meteoroids. The supply of Na and K by meteoroid bombardment has been discussed by Morgan et al. (1987). The vapor production depends on the mass and velocity of the object and the material properties of object and target surface. At velocities of 2 to 3 km s^{-1} or very small masses, the mass of vapor may be only a few percent of the projectile mass (Eichhorn 1976). Above 30 km s^{-1}, the mass of vapor may be many times the impactor mass (O'Keefe and Ahrens 1976). Vapor temperatures range from 2500 to 5000 K (Eichhorn 1978), and most of the sodium in the vapor should be atomic.

According to Lienert et al. (1981), the density of material varies with distance r from the Sun as $r^{-1.3}$. Fluxes at the Earth (Zook 1975), scaled to Mercury, predict a mean impact velocity near 30 km s^{-1} and a rate of 400 to 800 g s^{-1} for the whole planet. For a sodium content of 0.13% by mass, the source ranges from 1.4 to 5.6×10^{22} atoms s^{-1}; the highest figure assumes equal amounts of sodium from meteoroid and surface. If the Na/K ratio is 7 in the meteoroids and much greater in the crust, the potassium source ranges from 0.2 to 0.4×10^{22} s^{-1}. Because of the high temperatures, some of the sodium, and even potassium, atoms produced may be able to escape from the planet.

Meteoroids may be a much more potent source of water vapor than of alkalis. The meteoroid flux at the Earth could consist primarily of car-

bonaceous objects containing 10% water by mass, giving a source strength of 240×10^{22} s^{-1}. The photodissociation time at aphelion is 2×10^4 s (Kumar 1976), and the global average is twice as great; the resulting column density is 10^{11} cm^{-2} and the number density 2×10^4 cm^{-3}. The primary products of dissociation are H and OH, but some 13% of the events give H_2 and O (Gombosi et al. 1986). OH photolyzes rapidly, but may also adsorb to the surface and react with H or OH to recycle H_2O; if so, the effective lifetime and the abundance of the latter may be increased by a factor of ~8. Even without this effect, the sources of H and O would be 240 and 30, in units of 10^{22} s^{-1}. All of these estimates could be considered upper bounds, though we feel that they may actually be realistic.

Sputtering and Photodesorption. The most thorough discussion of these processes is that of McGrath et al. (1986); earlier work has been published by Potter and Morgan (1985*a*) and Ip (1986). In our terminology, McGrath et al. concluded that thermal evaporation is the most likely source of atmospheric atoms, and found that neither sputtering nor photodesorption is adequate. Here we look at their potential for generating source atoms. It should be noted that the second line of their Table 1 is mislabeled: it shows the incident flux, not the sputtered flux. The latter can be obtained by dividing the column densities N in the last line of their table by the assumed (ballistic) lifetime, 1000 s. Multiplication by the appropriate surface area gives the global production rates in Table V. For the ionic processes, we used the total surface area of the planet, 7.5×10^{17} cm^2; for photosputtering, this is divided by 4 to give the projected area.

A strong limit on the total rate of sputtering by all processes can be obtained from studies of lunar samples (McDonnell 1977; Carey and McDonnell 1978). This rate, 0.031 Å/yr (±30%) for the Moon translates to 0.19 Å/yr at Mercury's mean solar distance. If the total number density of Mercurian surface material is 8.9×10^{22} atoms cm^{-3} and the number fraction of Na is 0.002, the rate of sodium production is limited to 1.1×10^4 atoms cm^{-2} s^{-1}, or 0.8×10^{22} atoms s^{-1} for the entire surface. A fresh surface sputters much more quickly, but the rate settles down to the value given. Material richer in Na could produce a proportionally larger rate.

Processes that derive the sodium from the surface of Mercury are, in the end, limited by the rate of production of new regolith. On the Moon, the amount of new regolith typically deposited is 300 to 400 g cm^{-2} per Gyr (Langevin and Maurette 1978), corresponding to 1.9 to 2.2 m Gyr^{-1}. The process is not continuous and much of the material may be emplaced in a few episodes, particularly crater-forming events. Thus, the cratering record should be a good guide to the regolith turnover rate, and these records appear to be very similar for the Moon and Mercury (Murray et al. 1975; Wetherill 1975). Much of the material included in the estimates above is reworked surface material, so that a supply rate of "new sodium" calculated from the deposi-

tional rate is an upper limit. With 400 g cm^{-2} Gyr^{-1} and a sodium atomic fraction of 0.002, we find a maximum supply rate of 6.1×10^5 atoms cm^{-2} s^{-1} or, for the whole planet, 140×10^{22} atoms s^{-1}.

The supply rate estimated above for meteoroid influx is about 2 orders of magnitude smaller and therefore is not significantly affected by the upper limit.

C. Hydrogen and Helium

The global contents of hydrogen and helium were estimated in the previous section and appear in Table V, along with the source and sink rates discussed next. The deposition rates of solar-wind H and He P_{sw} follow the study of Goldstein et al. (1981), who suggest an uncertainty of about an order of magnitude. For their adopted solar-wind helium flux of 7.9×10^7 cm^{-2} s^{-1}, the quantity of He incident on a disk the size of Mercury is 1500×10^{22} cm^{-2} s^{-1}. Thus, the amount actually collected is around 1% of what it would be without the magnetic field. Goldstein et al. did not explicitly give numbers for H; those in Table V follow from their He/H ratio of 0.045.

Shemansky and Broadfoot (1977) suggest that the dominant loss process for helium is photoionization, because the high-energy tail of the thermal distribution is depleted. If so, the mean lifetime is at least the ionization time, $\sim 10^7$ s or 100 days, and the global loss rate is 11×10^{22} s^{-1}. However, ions may still return to the surface and be neutralized; Goldstein et al. (1981) suggest a loss efficiency β of 0.5, within a factor of 2 either way, and thus the minimum loss rate shown in Table V is 3×10^{22} s^{-1}. The estimated source and sink strengths are in reasonable balance, especially if β is fairly near 1. Semiannual or diurnal effects should be observable for helium, but the Mariner 10 observations were confined to aphelion.

The solar-wind source strength for H is several hundred $\times 10^{22}$ s^{-1}, and the likely source from photolysis of H_2O is comparable. Because the observed abundance is less than that of helium, and the ionization lifetimes are similar, the ionization loss rate is an order of magnitude less, and is 3 orders of magnitude smaller than the source. Some loss of atomic hydrogen may be driven by solar radiation pressure (Smyth 1986), but again the small densities argue against a large effect. Only two alternatives remain: thermal escape and chemical combination into an unobservable molecule such as H_2, unless there is a large loss of source atoms.

Another possible source of H is photolysis of H_2O, suggested by Broadfoot et al. (1976) as an explanation of the cold component of Fig. 3. The required number density of H_2O would be 2×10^6 cm^{-3} for a loss rate assumed to be 1000×10^{22} s^{-1}. The H_2O amount suggested above is 2 orders of magnitude less. If the lifetime of the cold H is increased by this factor, the mechanism could be viable.

Direct use of the Jeans equation with the 420 K component of Fig. 3 gives a lifetime of 10^4 s and a loss rate of 80×10^{22} s^{-1}. On the unlikely assumption that a similar lifetime would apply to the cold component, which

has twice the abundance (Table I), the thermal sink still does not seem adequate. Any *ab initio* estimate of thermal loss must include a computation of the velocity distribution, which has not been done. The distribution must be even more distorted than that for He (Fig. 14), which is itself uncertain. Of course, freshly released ("source") atoms may escape immediately, if they are directed upwards.

Even with the maximum likely thermal loss rate, the supply of H seems to exceed the loss by a factor of 3, and a much larger factor seems possible. Similarly, Hodges (1973*b*), comparing the lunar observational upper limit for H with a value based on his model (which is severely criticized above), concluded that there is a severe depletion. He suggested formation of molecules such as H_2. Thomas (1974) suggested H_2O, as explaining the deficiency. The molecules H_2, He, CH_4 and H_2O have been identified in the lunar subsurface as produced from the solar wind (Gibson 1977). Surface grains contain a large quantity of implanted H, and although the details are obscure, the formation of H_2 seems inevitable.

A rough upper bound to the expected H_2 density can be estimated by scaling from He, and by assuming that in steady state nearly all of the incident H is released from the surface grains as H_2. The ratio of the photoionization times is 0.21 (Kumar 1976), and photodissociation is much slower. The dayside density should therefore be $\sim 10^4$ cm^{-3}, and the nightside enhancement similar to that for helium. If thermal or nonthermal escape is significant, as it could well be, this estimate would be reduced. For CH_4 and H_2O, much smaller abundances would be expected for two reasons: small solar-wind fluxes of C and O (about 10^{-2} that of He), and short lifetimes against photodissociation. In principle, the surface silicates offer an additional source of O, but it seems likely that the available atoms have long since been used up. Densities of 1 cm^{-3} or less seem reasonable.

D. Sodium, Potassium and Oxygen

Although it is likely that all of the constituents vary with time, available observations are limited to sodium (Potter and Morgan 1987). Significant night-to-night variations appear to occur, and there is little doubt that variations occur on a 100-day scale. These are consistent with the time scale of a few days associated with photoionization.

Sources. As discussed above (Sec. VI.B) and summarized in Table V, there are three major candidates for the principal sodium source: ionic sputtering, photosputtering, and meteoroid impact. Unless the limit from the lunar erosion rate derived above in Sec. VI.B (0.8×10^{22} s^{-1}) can somehow be refuted, the sum of the first two sources cannot exceed it, and meteoroids, at around 8×10^{22} s^{-1}, seem to dominate. However, the uncertainties are large enough that this conclusion could be upset.

The magnitude of the sodium production due to either photodesorption or impact vaporization is proportional to the elemental abundance of sodium in

the regolith, and calculations made to date have used very small values for the elemental abundance of sodium. The elemental abundance of sodium in the regolith of Mercury is often based on that of the lunar regolith which is quite small, and it is often argued that the temperature of the protoplanetary nebula was too hot in the region in which Mercury was formed to include any significant accretion of sodic silicates. Yet the Moon is clearly a less differentiated body than Mercury. Even if the global elemental abundance of sodium in a planetary body were small, differentiation may still concentrate that small amount into the crust. Thus, sodium is much more abundant in the crust of the Earth (over 2%) than in the planet as a whole. This is not to say that the abundance of sodium in the crust of Mercury is that high, but does say that 0.2% is a conservative number, and that an order of magnitude variation is possible due to the elemental abundance alone.

Sinks. With an escape fraction $\beta = 0.1$ adopted for the alkalis in Sec. VI.A, the loss rate for sodium due to photoionization is $60 \times 10^{22}\ s^{-1}$, larger by a factor ranging from 4 to 30 than the estimated meteoritic source. Several ways can be visualized to close this gap: a still smaller value of β; relaxation of the constraint on sputtering set by the lunar erosion rate; a larger meteoroid influx; or meteoroids richer in sodium.

Again, the discussion of sodium can be adapted to potassium, with the somewhat different numbers shown in Table V.

The presence of *atomic oxygen* has received almost no attention, perhaps because its presence was not announced until two years after the first Mariner 10 encounter (Broadfoot et al. 1976). Possible sources include sputtering by ions and atoms from the solar wind and photolysis of water vapor brought in by meteoroids.

E. Summary

The solar wind is the major source of hydrogen and helium in the atmosphere of Mercury, although a portion of the helium observed must be of radiogenic origin. Sodium, potassium and oxygen are derived from the surface or from meteoritic material. The sodium, in particular, may be converted from a cation in the regolith silicate assemblage by impact vaporization, or by photodesorption. Impact vaporization following meteoritic impact must be present, and provides a source of sodium and potassium in the event that the regolith is deficient in alkalis. Photodesorption will be a significant source if sodium can be supplied to the planet's extreme upper surface (to which photodesorption is limited). Charged-particle sputtering of surface materials may be the principal source of oxygen, but photolysis of water vapor is another possibility.

Loss following photoionization plays a major and possibly dominant role in the loss of helium, sodium, potassium and oxygen. The dominant loss mechanism for hydrogen is probably formation of molecules, but there are no

published rate calculations to show that formation of H_2 or H_2O in or on surface grains can account for the required rate of removal of hydrogen to attain a steady state. Loss of sodium and hydrogen due to radiation pressure may be important over portions of the orbit of Mercury.

The practical demonstration that the sources and sinks for any elements have been identified is that the calculated rates for addition and removal are in approximate balance. Our understanding of the following topics is still very incomplete:

1. The magnetosphere of Mercury;
2. The elemental and mineralogical composition of the regolith;
3. The meteoritic complex inside 0.5 AU;
4. Surface physics and surface chemistry.

That the desired balance has not been achieved for sodium, hydrogen and potassium may simply reflect this ignorance, rather than neglect of important sources or sinks. Carefully conceived observing programs may be able to test the importance of candidate sources or sinks for particular elements in the atmosphere. A better understanding of the atmosphere may provide valuable insights about many other aspects of the planet Mercury.

VII. INTERCOMPARISONS

A. The Moon's Atmosphere

Inspection of Table I does not reveal any large discrepancies between the atmospheric contents of the Moon and Mercury, given their vastly different distances from the Sun and different escape velocities. Although H was not detected on the Moon, the upper limit is similar to the density of the hot component on Mercury (cf. Fig. 3); it is a factor of 8 less than the cold component. Such a factor could be due to the greater solar-wind flux at Mercury, to absence of the cold component on the Moon, or to unsuitable geometry for detecting it. The helium contents of the two bodies are fairly similar. The landed experiments did not yield much information on diurnal variations, because they were swamped by gas from the payload and spacecraft on the day side.

The Moon has been observed with the same equipment that discovered sodium on Mercury, but no sign of emission has ever been found. It must be remembered that the intensity for the same amount of vapor tends to be two orders of magnitude smaller. Two effects each contribute about equally: the Moon-Sun Doppler shifts are always small, and the distance from the Sun is large.

All of the physical processes that might work to add or remove the constituents of the atmosphere of Mercury are also at work on the Moon. While the rates are different, they can, in principle, be calculated with much more

certainty for the Moon than for Mercury. The Moon's surface composition is known, and the particle and field environment has been determined. The meteoroid flux, the velocity distribution of the meteoroids, and the elemental composition of the meteoritic material are also known at 1 AU. In short, a model of the atmosphere of Mercury can also be adapted to make predictions about the atmosphere of the Moon.

B. The Earth's Atmosphere

A very large amount of literature exists on observations and interpretations of alkali metals, especially sodium, which appear as a layer in the mesopause region, at an altitude of about 90 km. The layer thickness at half maximum is 10 km or less. The discovery of this layer (Bernard 1938) and subsequent study up to 1969 were carried out under twilight conditions, where the brightness of the sky is greatly reduced relative to the daytime, and height information can be obtained as the shadow of the Earth's limb scans through the layer (Chamberlain 1961; Hunten 1967). The corresponding dayglow was observed by rockets (Hunten and Wallace 1967; Meier and Donahue 1967). Lidar observations have been carried out more recently (see, e.g., Gardner et al. 1986), with similar results but a much better definition of the height profiles. A typical abundance is 3×10^9 atoms cm^{-2}, perhaps an order of magnitude smaller than is seen at Mercury. The sodium source is commonly believed to be meteoroid ablation, which reasonably explains the observed densities if the sodium content is a few percent (Gadsden 1968; Hunten 1984).

The presence of free sodium is believed to stem from the large abundance of oxygen atoms in the upper atmosphere, through reactions of the type

$$NaO + O \rightarrow Na + O_2. \tag{9}$$

The cutoff at the bottom of the layer coincides with a large decrease in the density of O atoms; however, at and above the peak of the layer, the entire inventory of available sodium is expected to be in atomic form. Sodium ions can be detected by rocket-borne instruments, but are much less abundant than neutral atoms. The ions are certainly being produced rapidly, but are evidently recycled in some unknown way. The lifetime is probably limited by other processes such as deposition on dust particles, agglomeration into large aggregates and subsequent fallout. The rates of such processes are not well determined, but they are probably much slower than photoionization at Mercury.

A typical ratio of Li:Na:K is 1:8000:160, but it is variable with latitude, time, and season and its relationship to the sources is complex and obscure. This matter is further complicated by the presence of lithium injected by rocket experiments and, in the past, thermonuclear explosions. It is likely that the potassium source is the same as that of sodium.

Perhaps some day we will understand terrestrial sodium well enough to illuminate its Mercurian counterpart, but that day has not arrived.

C. Io's Atmosphere

Bright sodium emission from Io was unexpectedly discovered by Brown in 1973 and shown to be in an extended cloud to tens of Io radii by Trafton. Brown and Yung (1976) have provided a thorough discussion of the physics and of the first few years of observational results. There are many other reviews, the most recent that of Nash et al. (1986). Io, like Mercury, exhibits large changes in radial velocity which modulate the intensity of solar excitation by about an order of magnitude. Potassium is also present (Münch et al. 1976; Trafton 1977), and the Na/K ratio is 8 to 20.

Emission from ionized sulfur was discovered by Kupo et al. (1976). By the time of the Voyager encounter, it had been established that Io's orbit is surrounded by a sulfur torus with ion density of a few thousand per cm^3 and an electron temperature of ~50 eV. These results were confirmed and greatly extended by Voyager 1 (Broadfoot et al. 1979; Bridge et al. 1979); in particular, oxygen ions are also present, and the ratio of oxygen to sulfur is 2. Since SO_2 is a prominent constituent of Io's surface and atmosphere, it is impossible to avoid the suspicion that it, or its dissociation products, provide the major source of matter for the torus. The torus plasma, in turn, bombards Io and its atmosphere, producing collisions which are thought to create the major source of ions. Sinks are even harder to specify, although it is clear that ionization by electron impact is very important for neutral Na. In a second process, charge exchange converts corotating ions to fast neutrals that can escape the Jupiter system, but is not a net sink of charge. The third major process is magnetospheric radial diffusion.

Conditions at Io and Mercury are quantitatively very different. Io is bombarded by plasma ions at 55 km s^{-1}; Mercury is bombarded part of the time by protons and α-particles at hundreds of km s^{-1} and a much lower density. Io is immersed in Jupiter's strong magnetic field; Mercury has its own weak field and a very active regime of magnetospheric convection. It remains to be seen whether each has much to tell us about the other.

VIII. SUMMARY AND OUTLOOK

The persistent reader may have reached this point with an unsettled feeling. There are many open issues and many opportunities for further modeling and data interpretation. Work on the Mariner 10 results was broken off after 1978, with the encounters of Pioneer Venus and Voyager. The discoveries of sodium and potassium are so recent that they have not been fully assimilated, and there is plenty of scope for fresh work.

Nevertheless, a few statements can be made about the atmosphere of Mercury. The known gases H, He, O, Na and K are summarized in Table I. The surface number density of molecular hydrogen may approach 10^4 cm^{-3}, comparable to He and O. If argon can be scaled from the Moon, its density

would be a few hundred per cm^3. Nothing else is likely to exceed 1 cm^{-3}. The longer-lived and highly mobile gases He and perhaps H_2 and H should show nightside enhancements by a factor of around 50.

Capture of the solar wind is the probable source of hydrogen and helium, with an intermediate step of implantation, followed by displacement as further ions arrive. Ion sputtering or photosputtering probably eject oxygen from the surface, and must still be considered for sodium and potassium. For these latter two elements, however, impact evaporation of meteoroids seems more likely. Meteoroids may also be a large source of water vapor, which in turn supplies H, O and H_2. An important sink for all gases is photoionization and entrapment in the solar wind and magnetospheric flows, although it is likely that 90% or more of these ions are recycled to the surface. Thermal loss cannot be quantified at present, because the velocity distributions of the light elements are strongly non-Maxwellian, but may still be important for atomic and molecular hydrogen.

Transport across the surface, and speed and height distributions in the atmosphere, are strongly influenced by the nature of the atom surface interaction. Any adsorption to the surface lasts for times less than a second, especially on the day side; the typical collision is a scattering, not an adsorption. For helium, these collisions give an energy distribution that is highly deficient at high energies relative to a Maxwellian. This tendency is reinforced by escape of faster atoms. Similar effects are likely for hydrogen.

In the near future, several kinds of work could be pursued. Observation of the sodium and potassium lines can give information about temporal changes and spatial distributions. The Mariner data have much better spatial information, especially vertical distribution, than can be obtained from the Earth, and address lighter elements whose behavior is very different. Analysis of all of these data can benefit from further calculations of gas-surface interactions and migration over the surface; the results in Fig. 14 and Table IV represent only a start.

APPENDIX A: DEFINITION OF TERMS

The interdisciplinary nature of the study of the atmosphere of Mercury has led to some confusion in terminology. We therefore define terms used in connection with aspects of the subject encountered in this chapter.

Surface: The outermost layer of atoms of the solid component of the planet. This definition differs from that normally used in studies of solid geochemistry (see, e.g., Gibson 1977).

Sub-Surface: The region within ~500 μm of the surface.

Adsorption; physisorption: Physical-scale bonding of a gas atom to a surface

with a duration of at least one vibrational period. Bonding energies are <0.5 eV. In Fig. 13, the atom is oscillating in the potential well at r_e.

Adsorption; chemisorption: Chemical-scale bonding of a gas atom to a surface. Bonding energies are >0.5 eV.

Absorption or entrapment: Chemical-scale bonding of a gas atom in the subsurface.

Energy accommodation coefficient (α): Coefficient of fractional energy exchange of a gas atom with a surface, including both adsorption collisions and free-free collisions. The equation for α at the macroscopic level is defined by

$$\alpha = (E_2 - E_0)/(E_1 - E_0) \tag{A1}$$

where E_0 is the mean energy per atom of the impacting particle, E_2 is the mean energy per atom leaving the surface, and E_1 is the mean energy per atom in the limiting case of thermal equilibrium with the surface. Similar coefficients can be constructed to specify the fractional momentum exchange of gas atoms with the surface.

Sticking coefficient (S): Coefficient referring to chemical-scale bonding to the surface. The quantity S is the rate of adsorption per incident particle. The adsorption lifetime is undefined in the usage of this parameter, and it is therefore a useful quantity only for chemical-scale bonding in which residence time is long compared to typical experimental time scales. In the context of the present subject the sticking coefficient is generally not a useful quantity, and usage of the term can be unphysical and misleading.

Heat of adsorption (D_0): The dissociation energy measured from the zero-point energy level, which is somewhat higher than the minimum shown in Fig. 13.

Activation energy (E_a): Peak of the potential barrier above the separated atom asymptote, occurring at physical-scale internuclear distances; the minimum energy required for chemical reaction (see Fig. 13).

Exosphere, exobase: The outermost part of an atmosphere, in which collisions can be neglected to first order and the atoms can be regarded as executing ballistic orbits. Its bottom, the exobase, is taken as the level where the local mean free path is equal to the scale height. As emphasized in the text, there are important differences between a normal exosphere and an atmosphere like that of Mercury.

Ambient atoms: Atoms defined here as those atoms occupying the central box in Fig. 12; they include atmospheric atoms (defined next) and those adsorbed briefly to the surface.

Atmospheric atoms: Atoms actually in the ballistic atmosphere, with near-thermal energies.

Source atoms: Atoms freshly ejected from the surface or freshly generated in some other way, such as neutralization of an ion; in practice, distinguished from atmospheric atoms by their higher energies.

APPENDIX B: GAS-SURFACE INTERACTIONS

This Appendix gives some of the technical details behind the material in Sec. V.C. The residence time for adsorption is approximated by

$$\tau_{ad} = \tau_0 \exp (D_0/kT) \tag{B1}$$

where τ_0 is a vibration time for the van der Waals potential, around 10^{-13} s, and D_0/k is the heat of adsorption expressed as an equivalent temperature (see Fig. 13). With the values for helium shown in Table IV, the residence time at 200 K is found to be $\sim 10^{-12}$ s. The collision frequency, or flux to the surface, for an atmospheric number density n is

$$\nu = \left(\frac{kT}{2\pi m}\right)^{1/2} n \tag{B2}$$

which is $\sim 2 \times 10^{11}$ cm^{-2} s^{-1} at a nightside number density of 10^7 cm^{-3}. If the sticking coefficient is 1, the coverage is 0.2 atom cm^{-2}. Any approach to full coverage requires conditions not found on Mercury: namely pressure approaching one bar, temperature well below 100 K, or chemical bonding to give a much larger value of D_0. Observations of the day side imply mean energies corresponding approximately to the surface temperature, and there is no reason to believe that the "bonding" is other than physical.

Estimates of the heats of adsorption and accommodation coefficients depend on the composition of the surface material. Unfortunately we have no direct determination of surface composition, and it is necessary to resort to analogy with the Moon. The spectral reflectivities of Mercury and the Moon are very similar in shape and magnitude from infrared wavelengths to the EUV (McCord and Adams 1972*b*; Wu and Broadfoot 1977), and we assume similar surface compositions. The dominant surface materials on the Moon are calcium aluminum silicates and iron-rich silicates, although SiO_2 has been mentioned (Cadenhead et al. 1972). Calculations of gas-surface interaction characteristics have concentrated on the surface structure of quartz (Sheman-

sky and Broadfoot 1977; Kunc and Shemansky 1981). This is hardly an ideal situation, but is forced by the availability of the necessary laboratory information. There is some justification in that one important quantity is the Debye characteristic temperature, which depends mainly on the average atomic mass of the material.

The heats of adsorption of H, He, O, Na and K on α-quartz have been calculated by Kunc and Shemansky (1985) and Shemansky and Kunc (in preparation). These quantities are given in Table IV, along with crude estimates of accommodation coefficients. Table IV includes other basic physical properties required for a qualitative description of atmospheric characteristics, as well as for quantitative calculations. However, the accommodation coefficients (α) are based on classical theory and are not truly applicable to detailed calculation (Shemansky and Broadfoot 1977).

The kinetic energy distributions of the atmospheric gases on Mercury appear to be controlled by physical collisions with the surface. This argument is based on the observation that the mean energies of the particles are at most characteristic of the temperature of the solid surface. Source particles may however be involved in chemical-scale interaction, which may involve activation energies. If so, the dissociation process would typically provide energies in excess of 1000 K/atom (see Shemansky and Broadfoot 1977). The presence of gas essentially confined to the surface temperature then implies that the majority of interactions with the surface are on a physical scale.

Another approach to estimating the rate of adsorption on the surface of Mercury assumes an activation energy E_a which forms a small barrier. The flux (Eq. B2) is multiplied by the Boltzmann factor exp $(-E_a/kT)$ (Glasstone et al. 1941,p.351). No information is available on the size of such an activation energy, or even its presence; in this situation it is common practice to use the Hirschfelder semi-empirical rule

$$E_a \sim \frac{D_0}{20} . \tag{B3}$$

The Boltzmann factor does not differ much from unity unless $E_a > kT$, or $D_0 > 20\ kT$; even at $T = 100$ K, D_0/k would have to exceed 2000 K. For sodium it is about 3000 K, and the Boltzmann factor is ~0.2 on the night side. If we assume that the gas density at the surface on the antisolar side is ~100 times greater than observed on the day side, the number density $n(\mathrm{Na}) = 2 \times 10^6$ cm^{-3}. At $T = 100$ K, the downward flux at the surface is then $\nu(\mathrm{Na}) \sim 3 \times 10^{10}\ \mathrm{cm}^{-2}\ \mathrm{s}^{-1}$. The adsorption lifetime from Eq. (B1) is 0.7 s, and the areal density on the surface is $4 \times 10^9\ \mathrm{cm}^{-2}$, less than 10^{-5} of a monolayer ($\sim 6 \times 10^{14}\ \mathrm{cm}^{-2}$). Thus, it is almost certain that no significant part of the surface of Mercury is saturated in adsorbed gas.

This treatment assumes that the atoms are mobile in the adsorbed state,

which is only partially true for sodium with its relatively large value of D_0. The adsorption rate for immobile adsorbed atoms involves a concentration of activated sites denoted by [CS] (Glasstone et al. 1941,p.349). For sodium [CS] = 6×10^{14} cm^{-2}; the adsorption rate is given by

$$N[\mathrm{CS}] \frac{kT}{h} \frac{\omega_s}{F} exp \frac{-E_a}{kT} \tag{B4}$$

where

$$F = (2\pi mkT)^{3/2} \left(\frac{\omega_g}{h^3}\right) \tag{B5}$$

is the partition function per unit volume for the gas phase, h is the Planck constant, and $\omega_s = \omega_g = 1$ are the vibrational and rotational degeneracies of adsorbed and gas-phase atoms, respectively. With (B4) the adsorption rate is found to be reduced by about 2 orders of magnitude. The concentration of adsorbed Na given above is therefore an upper limit.

The rather long lifetime for Na on the antisolar surface does present an opportunity for formation of molecules. This possibility requires further research, and can only be discussed in a general way here. In the case of sodium and potassium on the dark surface of Mercury, the rate-limiting factors for combination reactions are the mobility and activation energy on the surface, rather than the adsorption lifetime. It is then possible to have reactions on the surface forming van der Waals Na_2 and K_2, and with a much lower probability, chemically bound versions of the same molecules. Two cases can be distinguished: reaction of two adsorbed atoms, and reaction of an incoming atom with an adsorbed one. If we assume a high mobility, a crude estimate of the rate of formation of van der Waals molecules from adsorbed atoms can be obtained (Glasstone et al. 1941,p.373):

$$N^2 \left(\frac{\sigma}{m}\right) \left(\frac{\pi}{kT}\right)^{1/2} exp \left(\frac{-D_0}{kT}\right) \tag{B6}$$

where σ is the atomic diameter. The result for the dark surface of Mercury is $\sim$300 cm^{-2} s^{-1}, a negligibly slow rate. The interaction of the downward flux with adsorbed atoms (of surface density N_{ad}) yields a similar rate:

$$NN_{ad} \left(\frac{kT}{h}\right) \left(\frac{\omega_s}{F}\right) exp \left(\frac{-E_0}{kT}\right) \tag{B7}$$

where E_0 is the activation energy for formation of van der Waals or chemically bound molecules. A suitable value for E_0/k is 100 K, which gives a formation rate of $\sim$200 molecules cm^{-2} s^{-1}. The effect of the formation of molecules

on the atmospheric distribution and loss rates is probably negligible, because the dissociation of chemically bound Na_2 or K_2 yields kinetic energy of ~0.2 eV (2200 K) per atom.

APPENDIX C: HELIUM ENERGY DISTRIBUTION

The energy distribution shown in Fig. 14 was obtained in the following way. The controlling factor for the helium atoms is the heterogeneous collisions with the surface. The collisionally equilibrated system can be described by the general expressions, Eqs. (C.1) and (C.2)

$$P_{ij} = v\sigma_{ij}n(E)dE \tag{C1}$$

where P_{ij} represents the probability per solid population element s_i in level i for excitation to level j by collision with the helium population in the energy range E to $E + dE$, $n(E)$ is the differential population distribution of helium atoms, v is the collision velocity, and σ_{ij} is the excitation cross section.

$$L_{ji} = v\sigma_{ji}n(E)dE \tag{C2}$$

is the deactivation probability per solid population element s_j in level j for a reciprocal transition to level i, and σ_{ji} is the cross section for the deactivation process in the solid population. As a matter of convenience, the cross sections σ are related to the collision strengths Ω_{ij} defined by

$$\sigma_{ij} = \frac{h^2}{4\pi m v^2}\frac{\Omega_{ij}}{\omega_i} \tag{C3}$$

where m is the atomic mass, and ω_i is the degeneracy of level i. The principle of detailed balance, which defines a thermodynamic equilibrium, requires each microscopic process to be balanced by its inverse. A necessary condition for this principle is that

$$\Omega_{ij} = \Omega_{ji}. \tag{C4}$$

As a consequence, in thermodynamic equilibrium, the collision strengths, which contain the energy-dependent physical properties of the reactions, cancel out in the equations of equilibrium (such as the Saha equation). In thermodynamic equilibrium, no knowledge of the physical properties is required to define the populations of the excited states.

In the case of interest here, the ratios represented by Eqs. (C1) and (C2) are exceedingly small relative to reactions in the solid and the rates in the equilibrium established by radiative balance with solar input and conduction

between the surface and the subsurface. The vibrational populations s_j in the solid therefore have no dependence on the atmospheric atoms, whereas the differential energy distribution $n(E)$ depends on collisional coupling to the solid. The much larger rates for gas-solid collisions relative to homogeneous rates then place control of $n(E)$ on the population distributions s_j and the physical properties of the energy-dependent collision strengths Ω_{ij}. The distribution of populations in the solid cannot adjust to produce detailed balance with the gas, in analogy to the collisionally excited ion populations in a low-density plasma. Here the populations are controlled by radiative loss rather than by detailed balance with the electron population (see, e.g., Osterbrock 1974).

The calculation illustrated in Fig. 14 is based on collision strengths $\Omega_{ij}(E)$ derived from the one-dimensional theory of Devonshire (1937) which describes the collision process for light gas atoms as being dominated by single-phonon events. The general characteristics of the interaction are summarized by Shemansky (1980).

Note added in proof: Sodium and potassium in the lunar atmosphere have been observed by Potter and Morgan (1988) and the sodium also found by Tyler et al. (1988). Near the subsolar point, the two groups find essentially identical number densities for sodium, 50 to 60 cm^{-3}, and the Na/K ratio is between 3 and 9. The sodium scale height is consistent with the surface temperature. The ratio of sodium densities on Mercury and Moon is therefore around 400, much greater than any likely ratio of meteroid impact fluxes. Potter and Morgan suggest a reduced loss rate for Mercury, probably due to its magnetic field, while Tyler et al. favor an increased source strength, suggesting that Mercury's interior is warm enough to permit diffusion of sodium atoms to the surface.

References

Potter, A.E. and Morgan, T.H. 1988. Discovery of sodium and potassium in the atmosphere of the Moon. *Science*, in press.

Tyler, A.L., Kozlowski, R.W.H., and Hunten, D.M. 1988. Observations of sodium in the tenuous lunar atmosphere. *Geophys. Res. Lett.* 15, in press.